Development and Characterization of an Advanced Holographic Instrument for Atmospheric Research

Susanne Glienke[1*], Kevin L. Bertschinger[2*], Fan Mei[1], Eduardo Rodriguez-Feo Bermudez[1], John Shilling[1]

[1] ~~Atmospheric, Climate, and Earth Sciences~~ Integrated Discovery Sciences Directorate, Pacific Northwest National Laboratory, Richland, WA, 99352, USA
[2] National Security Directorate, Pacific Northwest National Laboratory, Richland, WA, 99352, USA

Correspondence to: Fan Mei (fan.mei@pnnl.gov), Bertschinger, Kevin L (kevin.bertschinger@pnnl.gov) ~~Susanne Glienke (susanne.glienke@pnnl.gov)~~

*SG and KB contributed to this manuscript equally.

Abstract.

In this study, we develop and characterize an advanced holographic instrument — HOLODROPS (HOLOgraphic DROPlet Sensor) ~~— along with a complementary event-based Particle Image Velocimetry (ePIV) system~~. HOLODROPS operates in two configurations: (1) HOLODROPS, designed for long-term, high-precision measurements of cloud droplet size distributions, and (2) HOLODROPS-TRACK, designed for targeted, short-interval particle tracking to study turbulence and collision-coalescence processes. Unlike traditional optical scattering or imaging probes, both configurations can simultaneously capture the size, shape, and three-dimensional position of multiple droplets and ice crystals larger than 8.8 µm within a sample volume, eliminating the need for multiple instruments and yielding more accurate and cohesive data. However, the detailed three-dimensional particle tracking provided by HOLODROPS-TRACK requires significant computational resources for hologram reconstruction and data processing, limiting its use over extended measurement periods. To address this challenge, we developed ~~the~~ a complementary event-based Particle Image Velocimetry (ePIV) system, which leverages an event-based camera to assess key cloud motion features in real time with substantially lower data volume and processing. ~~By rapidly characterizing the flow conditions~~, ePIV ~~is a complementary system that can identifies~~ provides continuous monitoring of ~~fluids~~fluid flows to ~~find~~identify optimal measurement windows and ~~informs~~ triggers targeted ~~manual~~ deployment of HOLODROPS-TRACK, paving the road for efficient, high-resolution particle tracking when conditions are most scientifically valuable. All three systems have been successfully characterized and validated in the laboratory. Additionally, we ~~tested HOLODROPS successfully in an outdoor setting with~~successfully tested HOLODROPS in an outdoor setting during a drizzle event to demonstrate the adaptive operation of the prototype.

Short Summary

Knowing accurate cloud droplet size distributions and droplet ~~movement is important to understand~~motion is important for understanding cloud formation and lifetime. To better measure these, we developed and tested the HOLOgraphic DROPlet Sensor (HOLODROPS) with two operational configurations, which can be used for both long-term cloud measurements and

for short-term droplet tracking, ~~in conjunction with~~ aided by an event-camera-based Particle Imaging Velocimetry (ePIV) system for ~~fast analysis of~~ optimizing droplet ~~movements~~movement capture.

1 Introduction

The study of atmospheric processes is intricately linked with the advancement of instrumentation, as cutting-edge tools are essential for ~~unravelling~~ unraveling the complexities of the atmosphere. Especially clouds still contain many secrets that we need to uncover to fully understand the underlying processes, and to improve both weather and climate predictions. To understand, for example, why some clouds rain~~, and others do not, we need to be able to know the internal structure of the clouds and the droplet size distributions accurately, which can only be done with measurements by deploying the high precision~~ and others do not, we need to accurately determine the internal structure of the clouds and the droplet size distributions, which can only be done with measurements using high-precision instruments in a cloud chamber or a real cloudy environment. Knowing the size distribution of cloud droplets helps explain precipitation since this depends on how liquid water is distributed among droplets. For example, smaller droplets of similar size have the same velocity and rarely collide. While a broader distribution with larger droplets, then these droplets can collide through ~~collision-coaliscence~~collision-coalescence, and once these droplets get large enough ~~can~~ to form drizzle (Lu et al., 2018).

Generally, advanced techniques can be divided into in-situ and remote sensing methods. For in-situ meas~~urements, either airborne or on mountaintops, the instrument is exposed to the cloud and measures directly the size, number of~~ concentration and sometimes phase of the ~~droplets~~hydrometeors. Typically, individual droplets are measured, and a size distribution is determined after averaging over time. Counting statistics are typically ~~high enough to get~~sufficient to obtain meaningful size distributions within one second. This means that for an airborne instrument flying at 100 m/s, averaging over 100 m, and even for a ground-based instrument, the cloud can change significantly within that time.

For in-situ instruments, there are two main techniques used~~,~~: scattering, holographic, or shadow imaging. Shadow imaging, as the name suggests, uses shadow images to determine the size and shape of each ~~individual hydrometeor, and counts~~hydrometeor and to count them to obtain a size distribution. Holographic uses a coherence light source to illuminate particles~~,~~ and capture the interference wavefront. For scattering, Mie theory is used ~~(Lance et al., 2010):~~ (Lance et al., 2010). A droplet scatters light at a predetermined angle at a known intensity and thus can be sized when that intensity is measured. Again, individual droplets are measured to obtain the size distribution. Furthermore, there are techniques that determine the bulk properties of clouds, such as liquid water content.

~~Remote sensing instruments are typically ground- or space-borne instruments measuring a bulk of the cloud simultaneously. However, often for RADAR or satellite observations a droplet size distribution shape is already assumed, and individual droplet properties are not determined. Also, the measurement is over a large area and thus averages in space.~~ Remote sensing methods infer particle size distributions (PSDs) indirectly by measuring how aerosols, cloud droplets, ice, or precipitation

scatter, absorb, emit, or reflect radiation. Active radar transmits microwave or millimeter-wave signals and measures the ~~returned signal; single-frequency radar mainly provides reflectivity, which is strongly weighted toward larger particles, while multi-frequency radar uses differences between wavelengths to better constrain~~ return signal; single-frequency radar primarily provides reflectivity, which is strongly weighted toward larger particles, whereas multi-frequency radar uses wavelength differences to better constrain the characteristic particle size and PSD shape. Doppler and polarimetric radar ~~add information about particle fall speeds, shapes, orientation, and hydrometeor type~~provide information on particle fall speeds, shapes, orientations, and hydrometeor types, improving PSD estimates for rain, snow, and ice. Passive methods, such as visible/near-infrared satellite imaging, thermal infrared sensing, microwave radiometry, sun photometry, and polarimetry, use natural solar or thermal radiation to estimate quantities like aerosol optical depth, cloud optical thickness, effective radius, liquid or ice water path, and fine/coarse aerosol modes. Overall, active methods generally provide more direct vertical and size-sensitive information, while passive methods offer broad spatial coverage but usually retrieve averaged or column-integrated PSD properties rather than ~~a~~the full size distribution.

1.1 Currently available cloud droplet measurement instruments

Due to the importance of accurate measurement of cloud droplet size distributions, several instruments and techniques have been developed for a variety of applications and size ranges. A popular method for measuring droplet sizes up to 50 ~~um in-situ is using the amount of light scattered to determine the~~ μm in situ is to use the amount of light scattered to determine droplet sizes following Mie theory. Examples of these type of instruments are the Cloud Droplet Probe (CDP, (Lance et al., 2010)), the Fast Cloud Droplet Probe (FCDP) and the Forward Scattering Spectrometer Probe (FSSP/FFSSP, (Pinsky and Khain, 2001)), as well as the Polar Nephelometer. The Phase Doppler Particle Analyzer (PDPA) uses the Doppler shift of scattered laser light to measure the velocity and size of cloud droplets. A relatively new technique that uses interferometry to measure the size and velocity of cloud droplets is the Interferometric Mie Imaging Probe (IMIP), providing high-resolution, high-speed measurements and can measure droplets as small as 1 μm ~~um~~ in diameter. Shadow imaging and direct particle imaging is another common technique; instruments either get triggered by a passing particle (e.g., Cloud Particle Imager (CPI)) or scan a passing particle as it passes through the sample volume (e.g., Two-Dimensional Stereo Probe (2DS), High Volume Precipitation Spectrometer (HVPS), Cloud Imaging Probe (CIP)). These instruments measure larger particles, with the ~~smallest reliable~~smallest, reliable size ~~ranges from 20 um, and can potentially differentiate between ice crystals and liquid~~droplets~~s~~range from 20 um, and can potentially differentiate between ice crystals and liquid droplets.

The aforementioned instruments all measure one particle at a time~~, and therefore results need to be averaged over time or space to give statistically relevant~~; therefore, results need to be averaged over time or space to yield statistically meaningful results. For bulk in-situ measurements~~, there are instruments such as the Hot-wire Liquid Water Content (LWC) Sensor (Strapp et al., 2003), measuring the~~instruments such as the Hot-wire Liquid Water Content (LWC) Sensor (Strapp et al., 2003) measure LWC by heating a wire and measuring the cooling effect of evaporating droplets. Similarly, the Particle Volume Monitor

(PVM) measures bulk LWC by analyzing the light scattered from an ensemble of droplets. None of these instruments can give information about individual droplets.

Holographic Measurement (e.g. (Fugal and Shaw, 2009)) combines the individual droplet measurements with the benefit of bulk measurements. ~~Holography~~Holographic reconstruction is able to determine the size, shape, and 3D position of each particle providing droplet variability, detect nonspereical particles, identify clusters, and produce detailed size distributions. In conjunction, thousands of droplets can be measued over time which can provide bulk ~~quanties~~quantities such as particle size distribution, number concentration, liquid water content, and spatial variability (Baumgardner et al., 2011). It is a relatively rarely used technique for cloud droplet measurement, and involves using a laser to create a hologram of a volume of cloud, which can then be reconstructed to give three-dimensional information about the location of droplets in space, and two-dimensional images of the cloud droplets. This allows for the measurement of droplet size, shape, and concentration, as well as the spatial distribution of droplets within the cloud. ~~Holography has the advantage of being able to capture a large volume of cloud at once, and it can measure droplets ranging from a few micrometers to several millimeters in size. However, it's a technique that generates a large amount of data, requiring large computational power for data analysis.~~

~~The largest drawback for a vast majority of methods is the need for airflow and the accurate knowledge of it. In airborne applications, the aircraft speed is much higher than the negligible amount of natural air flow, which is why these methods work so well. In a laboratory setting, such as within a cloud chamber, or in stationary measurements such as on a mountaintop however, airflow is very small and not well known. Only if there is airflow induced (such as an outlet for droplet sampling), these methods can be used. However, an induced airflow will impact the turbulence and other physical processes and is therefore not desired. Holography does not require air flow and is therefore the ideal candidate for our application.~~

1.2 ~~1.2~~ Review of holographic techniques

Holography has the advantage of being able to capture a large volume of cloud at once, it can measure droplets ranging from a few micrometers to several millimeters in size, and can capture complete droplet size distribution from a single hologram. To is possible, since holographic imaging provides a large depth field compared to a focal point or laser sheet with other techniques. The large sample volume can be 10 cm^3. However, it's a technique that generates a large amount of data, requiring large computational power for data analysis.

The largest drawback ~~for a vast majority of methods is the need for airflow and the~~ of the vast majority of methods is the need for airflow and accurate knowledge of it. This is important to avoid resampling a stagnant volume, and precise aspiration speed ~~are needed to calculated~~is needed to calculate concentrations. n airborne applications, the aircraft speed greatly exceeds the negligible natural airflow, which is why these methods perform so well. In a laboratory setting, however, such as inside a cloud chamber, or in stationary measurements, such as on a mountaintop, the airflow is comparatively small and poorly characterized. These methods can therefore only be applied if airflow is deliberately induced, for example through an inlet for droplet

sampling. Such induced airflow, however, perturbs turbulence and other physical processes and is thus undesirable. Holography requires no airflow at all, making it the ideal candidate for our application.

~~,comparablyinduced airflow will affect turbulence and other physical processes and is therefore undesirable~~

Formatted: List Paragraph, Indent: Left: 0.25"

Conventional cloud instrumentation, described above, measures single droplets at a time. In contrast to that, holography can measure a large sample volume (cm^3) at a single time with thousands~~many~~ droplets inside . Thus, there is no need for airflow, making this technique perfect for a chamber setting. Therefore, the need to average over time is not given, and the cloud structure can be examined on a within a few collected holograms~~very small scale~~. Holography can detect the size, number concentration, phase and spatial distribution of a large number of droplets at one time. These instruments provide valuable information about cloud droplets and can be used in conjunction with other methods to get a more complete picture of cloud properties. However, holography is a complex technique that requires sophisticated equipment and data analysis.

1.2.1 Existing holographic instruments

Most of the existing holographic instruments are designed for a mobile deployment either on aircraft, balloon or gondola, and are therefore somewhat restricted in the sample volume; a summary with key properties can be found in Table 1. The Holographic Droplet Sensor (HOLODROPS) presented here is designed for ground-based measurements of clouds and hydrometeors, ~~allowing for a larger sample volume and~~ more versatile deployments, such as in a laboratory setting (e.g. in a cloud chamber) or on mountaintop observatories. The system ~~can be~~was built on a ground-based platform that allows the distance between the laser and the imaging sensor to be adjusted, enabling it to capture a larger sample volume than mobile systems with fixed sensor spacing.

The current design has a variable sample volume that can be adapted to the desired circumstances. Furthermore, we ~~also developed HOLODROPS-TRACK, a system specifically designed for tracking particles in the same versatile environment, as well as ePIV (Event Particle Image Velocimetry) to complement the holographic measurements with instant~~developed HOLODROPS-TRACK, a system specifically designed to track particles in the same versatile environment, as well as ePIV (Event Particle Image Velocimetry) to complement the holographic measurements with instantaneous flow determination and optimize the capture strategy. This suite of capabilities fills a niche that the existing instruments are unable to cover, with high versatility, large sample volume and fast flow processing.

Table 1: Summary of existing holographic instruments.

Instrument	Developer	Resolution (μm)	Sample volume (cm^3)	Frame rate (Hz)	Platform	Pros	Cons / Development Challenges
HOLODEC	Michigan Tech / NCAR (Fugal and Shaw, 2009) (Fugal and Shaw, 2009; Fugal et al., 2004; Spuler and Fugal, 2011)	6-1000	13-15 cm^3	3-15	Airborne (aircraft)	Measures size, shape, and concentration; wide range (few µm to mm); well-established heritage with multiple publications	Requires aircraft deployment (costly); limited sample volume; averaging still needed for statistics
HALOHolo	University of Mainz (Schlenczek, 2017)	2.95	35.	6	Airborne (aircraft)	Larger sample volume than HOLODEC; higher frame rate	Still aircraft-dependent; similar complexity to HOLODEC; limited to airborne campaigns
HCP (Holographic Cloud Probe)	SPEC Inc.	10-12	N/A	N/A	Airborne (aircraft)	High-resolution 3D imaging of cloud droplets	Not commercially available; limited accessibility for the research community
HoloGondel / HOLIMO	ETH Zürich (Beck et al., 2017; Henneberger et al., 2013)	3.4	38	15	Ground-based (cable car, mountaintop)	Samples large cloud volume via cable car traverse; ground-based accessibility	Limited to locations with cable car infrastructure; not freely deployable; site-specific

Formatted: Centered
Formatted Table
Formatted: Centered
Formatted: Centered
Formatted: Centered
Formatted: French (France)
Formatted: French (France)
Formatted: French (France)
Field Code Changed
Formatted: Centered

Instrument	Developer	Resolution (μm)	Sample volume (cm^3)	Frame rate (Hz)	Platform	Pros	Cons / Development Challenges
HoloBalloon	ETH Zürich (Ramelli et al., 2020)	6	22.5	80	Balloon-borne	Unique in-cloud sampling perspective; can reach altitudes without aircraft	Limited payload capacity; tethered operation constraints; weather-dependent deployment
ICEMET	Finnish Meteorological Institute (Tiitta et al., 2022)	3-5	0.5	30	Ground-based (mountaintop)	Specializes in icing detection; expanding beam design	**Variable particle sizing accuracy** across sample volume due to expanding beam geometry; site-specific
HoloTrack	MPI-DS (Thiede et al., 2025b, a; Thiede et al., 2025c)	10	17	71	Airborne (kite)	Captures sizes, 3D positions **and** velocities; low-cost platform compared to aircraft	~~**Very small sample volume (~ 17 cm^3);**~~ limited by kite payload and stability

~~Table 1: Summary of existing holographic instruments.~~

1.2.2 Holographic techniques development/challenges

~~For a holographic system in a stationary setting such as a cloud chamber the components should be well chosen. However, a few trade-offs also have to be made between Lasers and camera options.~~ Designing a holographic instrument involves several choices that together determine overall system performance. A digital inline holographic system comprises two principal components: a camera imaging system and a coherent light source, typically a laser. The specific hardware selected and the geometry in which it is arranged directly affect holographic quality, and it is essential that the camera specifications be matched to the illumination properties. The key trade-offs are discussed in the following sections:~~When designing a holographic~~

Formatted: Centered
Formatted Table
Formatted: French (France)
Formatted: French (France)
Formatted: Centered
Field Code Changed
Formatted: French (France)
Formatted: Centered
Formatted: French (France)
Field Code Changed
Formatted: Centered

~~instrument there are several design choices that effect the overall system performance. Digital inline holographic systems consist of a camera imaging system, and a coherenct light source such as a laser. Different choices for hardware, and design will impact the holography quality, and it is essential to match up camera specification with illumination. The following trade off are discusses below.~~

1. Laser
    - Wavelength: Laser wavelength ~~e~~affects the diffraction of particle and the fringe spacing. Smaller wavelength ~~improve~~improves detectable spatial resolution of detected particles. ~~A good laser should have a small wavelength, since the wavelength is proportional to the smallest detectable particle.~~ This is why a UV laser is desirable. A visible (e.g. green) laser might also work, but if the same size particles should be detected, the optical magnification should be much larger.
    - Mode: A pulsed laser is needed to minimize motion blur when recording holograms with a slow-framerate camera imaging fast-moving particles. The short pulse freezes the motion by illuminating the sample volume for only an instant, capturing the particle interference pattern in a single frame. This effectively produces a sharp snapshot of the particles.
      Alternatively, a continuous-wave (CW) laser can be used if paired with a high-framerate camera operating at very low exposure times. Without sufficiently short exposures, CW illumination leads to blurred images or streaks due to particle motion, which is an important limitation in high-speed flows or when observing fast-moving cloud droplets.
    - ~~A pulsed laser is essential to the measurement method. A single short laser pulse illuminates the sample volume and all particles within, creating a hologram. Continuous lasers could be too long and streaklines would be measured, because camera exposure times are not short enough to compensate for the movement of the droplets. This is true for fast-moving droplets.~~
    - Energy~~.~~: The laser pulse energy must be sufficient to illuminate the full sample volume and produce detectable holographic fringes with adequate signal-to-noise ratio. The entire camera should be illuminated without dark edges. It should be high enough to account for sample volume length, beam size, optical losses, particle properties, and detector sensitivity, but low enough to avoid camera saturation, excessive background scatter, or particle disturbance. Uniform illumination is also important to minimize spatial bias in particle detection. ~~The laser should have enough energy to illuminate the entire length of the chamber. If a dual system is built for particle tracking, the volume has to be illuminated simultaneously, which would require one laser and a beam splitter. This would reduce the power of the laser for each system.~~
2. Camera options with pros/cons
    - Speed: ~~The camera speed is not very important, because the exposure time is mainly dependent on the laser pulse width, which is much shorter. However, for fast-moving droplets the camera and laser have to be matched such that only one pulse per image is recorded. If the camera and laser are not matched and the~~

~~droplets move fast, there is a potential for multiple imaging of the same droplet in the same frame. Alternatively, a continuous laser can be used if the exposure time is small enough to not capture particle motion blur.~~ As previously mentioned the Camera frame rate should be match with the illumination source. When using a pulse laser source the camera acquisition and laser trigger must be synchronized so that each frame records only one laser pulse. If multiple pulses occur during a single frame, fast-moving droplets may appear multiple times in the same hologram. If using CW illumination, then the camera exposure time should be short enough to keep particle displacement below the allowable motion-blur limit.

- Pixel size: The ideal pixel size is as small as possible, so small particles can be detected. The minimum size particle to be detected is two pixels in diameter; below that it is too uncertain and could be noise (Henneberger et al., 2013; Kaikkonen et al., 2020). The pixel size and the number of pixels determine the overall size of the focal plane array, which in turn sets the achievable sample volume. This ultimately limits how large a sample volume can be used in practice.
- Detector size: Detector size should be as large as possible to capture a large sample volume.
- Frame rate: Frame rate is a trade-off: For particle tracking, a high-speed camera is necessary to capture the same particle many times in the same frame. However, these cannot run for hours, and even if they could, too much data that cannot be processed currently, would be recorded. So, we aim for two sets, one low frame rate camera that can record for many hours and gives us an idea of what the conditions in the chamber are, and a system with two high-speed cameras for particle tracking.

Instrument	Lens system	Wavelength (nm)	mode	pixel pitch (um)	sized	sample volume (cm^2)
HOLODROPS	lensless	355	pulse	3.45	6480x4860	106
HOLODROP-TRACK	lensless	532	CW	4.5	4096x2160	57
ePIV	Fixed focus	532	CW	4.86	1280x720	10

Formatted Table

A holographic instrument is crucial for atmospheric research because it provides comprehensive and high-resolution measurements of cloud droplets, enabling a deeper understanding of cloud microphysics and dynamics.

As outlined above, holographic instruments such as HOLODEC, HALOHolo, HoloGondel, and others have demonstrated remarkable capability in simultaneously capturing the size, shape, three-dimensional position, and concentration of cloud droplets within a sample volume — a feat that conventional single-particle probes cannot achieve. Beyond these static

microphysical properties, holography also offers the unique potential to track the movements of individual droplets across successive hologram frames, enabling direct observation of particle velocities, turbulence-driven relative motion, and even collision-coalescence events as they occur. However, this tracking capability comes at a ~~significant~~ higher cost: holographic reconstruction is a complex technique that requires sophisticated data analysis, and extracting full three-dimensional trajectories from dense hologram sequences demands substantial computational resources and processing time. This creates a fundamental tension — while holographic tracking can provide unparalleled microphysical detail, it is impractical to apply continuously over extended measurement periods or across large datasets.

1.3 Particle Image Velocimetry (PIV) and Particle Tracking Velocimetry (PTV) Methods

Particle Image Velocimetry (PIV) offers a complementary path forward. It is a widely-used technique for measuring fluid flows (Willert and Gharib, 1991). Unlike Particle Tracking Velocimetry (PTV), PIV adopts a Eulerian approach, providing a macroscopic description of velocity at multiple points in space. This generates vector fields offering a detailed representation of the fluid flow over an area of interest. PIV is particularly robust in delivering dense, instantaneous velocity fields for a defined interrogation region and is well-suited for applications involving high particle concentrations.

On the other hand, PTV provides insights into individual particle movements, making it ideal for capturing complex dynamics, such as transient phenomena and rapid changes in flow behavior (Lu et al., 2008). In essence, PIV and PTV are complementary techniques for studying fluid flow dynamics: PIV offers an overarching view of particle flows, while PTV emphasizes individual particle trajectories.

Both Particle Tracking Velocimetry (PTV) and Particle Image Velocimetry (PIV) are highly suitable techniques for characterizing clouds, with cloud droplets serving as effective tracer particles. PTV specializes in tracking individual particles, measuring their velocities, and capturing droplet dynamics such as growth, ice crystal formation, aggregation, coalescence, and collision processes. On the other hand, PIV excels in providing flow characterization, assessing turbulence, spatial averaging, and identifying fluid currents, including phenomena such as evaporation and condensation.

In this study, to evaluate the PIV setup, a spray nozzle was employed for measurement and characterization. The spray nozzle generates inherently turbulent and chaotic fluid flows, and was aligned to direct particle motion primarily along the x-axis. This configuration facilitated testing of instantaneous velocity fields and enabled the determination of average velocity fields. Because the event–based camera responds only to changes in pixel intensity, it captures fluid motion efficiently. Its low latency resolves fast–moving flows, while the sparse output reduces ~~the~~ overall data bandwidth. The camera also operates at low power over a USB connection, which allows velocity fields to be displayed in real time during acquisition. The high speed camera used for HOLODROPS-TRACKS requires up to 75 W and an external trigger to begin recording. Its high data rate means that frames are written to an onboard buffer, which must then be offloaded to a physical hard drive once acquisition is complete. HOLODROPS-TRACKS is delayed further by the holographic reconstruction required before velocities can be recovered. Table X summarizes the resulting differences in power, data rate, and time to a usable velocity estimate.

The remainder of this paper is organized as follows. Section 2 describes the development of the new holographic system, including two operational configurations, with a particle-tracking mode complemented by an ePIV setup. Section 3 presents the calibration, characterization, and validation of all three configurations, covering laboratory calibration and initial testing as well as a field deployment in an outdoor drizzle case. Section 4 summarizes the main findings and offers an outlook on future developments and improvements.~~In Section 2, we describe the development of a new holographic system, including an additional particle-tracking configuration and an ePIV setup. In Section 3, we present the calibration, characterization and validation of all three systems, outlining the calibration and initial testing in a lab setting and deployment in an outdoor drizzle case. We conclude Section 4 with an outlook on future developments and improvements.~~

2 Prototype Development and Instrument Description

2.1 HOLODROPS prototype

We developed two separate holographic configurations, HOLODROPS and HOLODROPS-TRACK. HOLODROPS is designed for long-term, high precision measurements of ongoing cloud conditions, while HOLODROPS-TRACK is meant to be operated in limited time frames to measure turbulence by tracking the individual particles in the sample volume. HOLODROPS uses a 31.4 megapixel machine vision camera (Prosilica GT6400, Sony IMX342), whereas HOLODROPS TRACK operates with an 8.3 megapixel camera (Kron Technologies, Chronos 4k12). In this paper, HOLODROPS is treated as the high resolution system, and it is referred to in that way throughout the text. In contrast, HOLODROPS TRACK employs a camera with lower resolution but much higher frame rates, making it the high speed counterpart to HOLODROPS

Due to these two ~~different~~ dis~~ff~~tinct purposes, the systems contain different components to maximize the benefits of each. The layout of both HOLODROPS and HOLODROPS-TRACK ~~are~~ is the same, and the setup for HOLODROPS-TRACK is shown in Figure 1~~Figure 1~~.

HOLODROPS contains a UV-laser (355 nm) and a high-resolution camera (3.45 µm ~~um~~ resolution), such that very small particles (>6.9~~6~~ um) can be imaged accurately. However, such a fine resolution limits the possible output of the instrument, which is 6 Hz maximum. The frame rate is therefore constrained by the focal plane array readout bandwidth, digitization electronics, and data-transfer capacity rather than by the laser pulse duration. The current design of HOLODROPS uses an enclosure for all components ~~that allows for~~, enabling safe laboratory operations. It is designed ~~modular such that the system can be adapted to a variety of laboratory situations, including varying the sample volume desired~~in a modular way so that the system can be adapted to a variety of laboratory situations, including varying the desired sample volume. While the enclosure itself is made ~~out of laser-safe materials, the optical path passes through windows made of uncoated calcium fluoride~~of laser-safe materials, the optical path passes through uncoated calcium fluoride windows. With this design the benefits of HOLODROPS become obvious; the variable sample volume that allows distances of several meters allows the use of

HOLODROPS with many different laboratory settings, including cloud chambers, as well as a flexible setup on ground-based observatories. The sample volume for HOLODROPS at 1 meter is approximately 3k cm^3.

HOLODROPS-TRACK contains a high-speed camera with 4.5 µm ~~um~~ resolution, in combination with a ~~contious~~continuous wave (CW) green laser (532 nm). It is intended to be operated in short time bursts when particle tracking is desired due to the large data bandwidth produced by this~~limits of the~~ camera operation. The highest data acquisition rate for this system is 1397 FPS at 8-bit.

Currently, the instrument can be deployed for brief periods of time outside, since it can be easily made water-proof. For extended outside operations, we plan to add heaters and cooling fans to keep the components at room temperature. We also plan to add a detector for times HOLODROPS should be recording, i.e. only when there is a cloud or precipitation, in order to limit the amount of data collected that has no droplets. For an outdoor deployment ~~on e.g. a mountaintop, HOLODROPS also needs to be easily aligned between the camera and laser, which we plan on having a mount between them, designed to minimize~~ , e.g., on a mountaintop, HOLODROPS also needs to be easily aligned between the camera and laser, which we plan to achieve with a mount between them, designed to minimize its influence on the airflow. Lastly, the instrument should always be pointed into the wind to reduce effects of shading of droplets as well as shattering/breaking of hydrometeors, and as such a wind vane would have to be added to the current design.

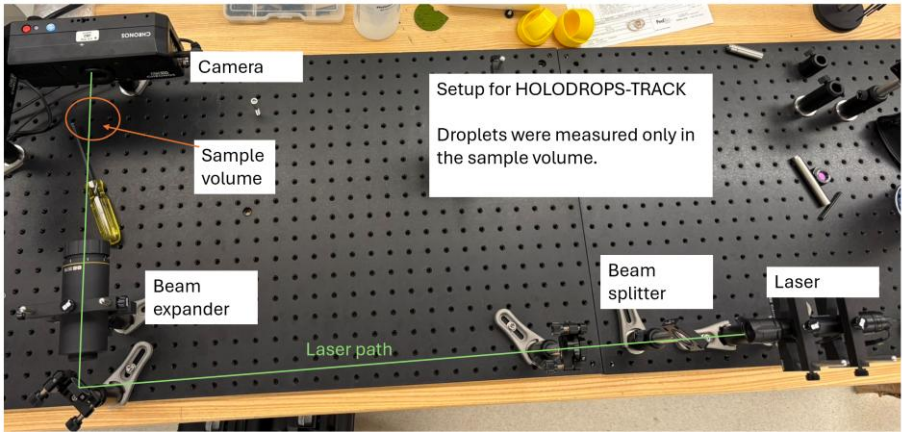


Figure 1: A prototype HOLODROPS, configuration for High-Speed Camera sampling, same setup used for High-Resolution sampling.

2.2 ePIV prototype

Experimental Setup for PIV Using an Event Camera

Neuromorphic event cameras operate by monitoring changes in the intensity of light at each pixel asynchronously rather than recording full image frames at fixed intervals. Every pixel functions independently and continuously checks whether the brightness it receives changes beyond a preset contrast threshold. When a significant change occurs, that pixel produces a positive event, and when the brightness decreases it produces a negative event containing its location, the exact time of the change. Because the sensor reports only meaningful changes, it generates a sparse stream of data that represents motion in a scene with remarkable temporal precision. This approach removes motion blur, reduces redundant information, and provides excellent performance in situations with rapid movement and high dynamic range {Gallego, 2020 #37}.

The event camera-based PIV system (ePIV) employs a continuous green laser (wavelength: 532 nm) to illuminate water droplets. A cylindrical lens is used to focus the laser light into a thin line along the z-axis, forming a thin laser sheet to illuminate the particles. A camera is carefully positioned and focused on the laser sheet at a distance of approximately 50 mm. Water droplets for testing are introduced into the setup using a nebulizer (Figure 2~~Figure 2~~).

In this experiment, an event camera serves as the imaging sensor. Event cameras, also known as neuromorphic cameras, are inspired by the functioning of the human eye. Instead of capturing traditional intensity-based images, they operate asynchronously, measuring changes in pixel intensity. This distinctive readout results in low latency and sparse data representation, with latency as low as 100 microseconds. Though event cameras do not record frames in the conventional sense, an equivalent frame rate would be comparable to 10,000 FPS (Gallego et al., 2020). In contrast, traditional high-speed cameras face bandwidth limitations as they capture full frames at high framerates. Event cameras overcome this limitation by only measuring changes, dramatically reducing the amount of data captured per frame. Additional advantages of event cameras include their lightweight design and lower power consumption compared to high-speed cameras. The event camera uses 1.5W of power while the high speed camera uses 75W of power. The event camera is 30x30x36 mm in size compared to the high speed camera which is 188x111x53 mm. The vent camera is 32 times smaller than the high speed camera, and requires 50x less power to operate.

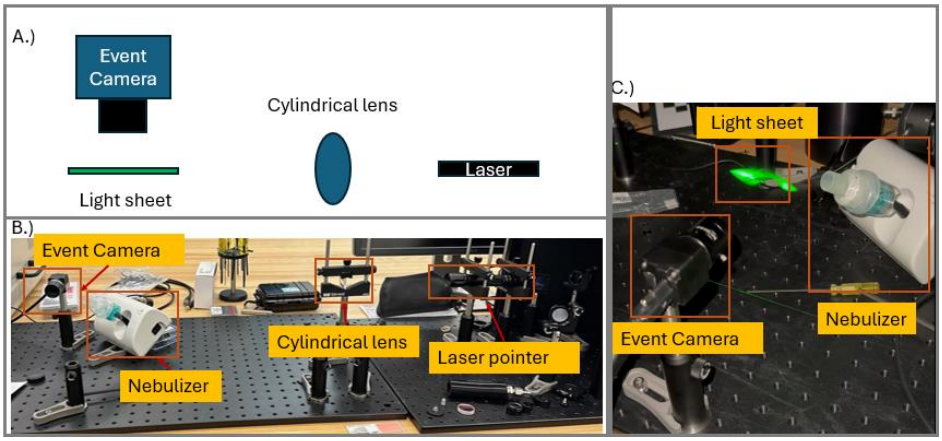


Figure 2 A.) Typical PIV set up. B.) Side view of the experimental setup. C.) image of the water droplets illuminated by the laser.

Event Cameras for Fluid Flow Imaging

Event cameras are highly effective at imaging fluid flows due to their ability to inherently measure changes in pixel intensity (Willert and Klinner, 2022). This characteristic allows for the automatic detection of particles within a frame, eliminating the need for manual thresholding and significantly streamlining the analysis process. Furthermore, the low latency of these cameras enables the detection of particles at high speeds, making them ideal for dynamic imaging applications.

Unlike standard cameras that capture entire frames, event cameras record only changes in pixel intensity, focusing solely on alterations within the scene. This approach minimizes redundant information and significantly reduces data bandwidth requirements. For instance, fluid flows captured from the nebulizer are efficiently visualized using this technique.

To facilitate analysis, the event data is transformed into pseudo-frames over fixed time intervals. This conversion ensures compatibility with open-source Particle Image Velocimetry (PIV) software (Shirinzad et al., 2023). In this study, the openPIV package was utilized, which applies cross-correlation methods within defined interrogation windows to calculate fluid velocity fields across different spatial regions (Willert and Gharib, 1991).

3. Calibration, Characterization and Validation

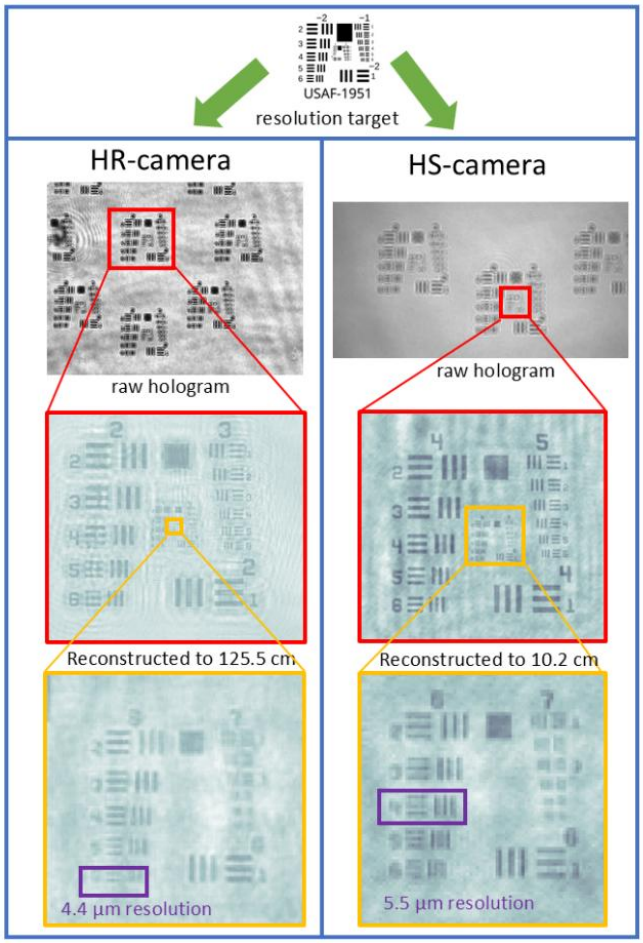
~~The calibration and characterization is~~Calibration and characterization are very important to ensure accurate measurements in the future. Therefore, we measure the effective size of individual pixels of the system, its efficacy and accuracy in processing in a few different ways. These are done under controlled conditions in the laboratory, to determine the possibilities of the

instrument in ideal conditions. First, we use a USAF1951 resolution target to determine the effective pixel size at various distances and to determine the best distances between camera and laser. Then, we use calibration glass beads of known sizes to confirm with more realistic shapes. Synthetic holograms were used to determine the accuracy of the particle detection and tracking methods. Lastly, we used a nebulizer to confirm how water droplets are seen and detected by the system.

3.1 Resolution target

Formatted: Heading 2

We used a USAF1951 resolution target in the sample volume of both systems to verify the effective pixel sizes. This target has patterns of three horizontal and vertical lines of various sizes, and the smallest completely resolvable pattern shows the resolution of the system (Figure 3). The resolution of the HR camera system is as expected, with a 4.4 µm resolution at a distance of 125.5 cm. This means that features of 4.4 µm can be resolved at this large distance, and even more conservative approaches of twice the resolution will yield detectable droplets of 8.8 µm diameter, and therefore below 10 µm, which we were aiming to achieve. The HS camera system was tested at a shorter distance since in real conditions it will also be closer to the objects to detect. It also performed really well, with a resolution of 5.5 µm; again, if twice this resolution is used, we can detect droplets at 11 µm, the size range we were aiming for.



Formatted: Centered

Figure 3: Resolution target results with both the high resolution (left column) and high speed (right column) camera

3.2 Glass beads

Formatted: Heading 2

To assess sizing accuracy for spherical targets across the droplet size range, dry borosilicate glass microspheres (Duke Standards) were introduced into the sample volume. The beads have NIST-traceable mean diameters of 14.4 ± 0.8, 29.5 ± 1.0, 42.3 ± 1.1 and 49.3 ± 1.4 µm, so the reference diameter is known to better than 3 % in all cases. As expected, the bead datasets are noisier than the droplet datasets, because residual dust from the atomizer and aerosol from the carrier flow are visible in the example holograms in Figure 4. Because the dry beads must be pneumatically introduced into the sample volume, the carrier jet introduces both particulate contamination and density gradients that act as a weak phase screen on the illuminating beam.~~To determine how accurate the sizing is for round objects in the size range of droplets, we use glass beads in the sample volume. The glass beads are of a known size, and the chosen sizes cover a range of size detections. In holography, glass beads will show the same as droplets in the data, and therefore can be used to simulate droplets of an exactly known size.~~

For the high resolution camera system (1 pixel = 3.45µm), the 14.4 (15), 29.5 (30) and 49.3 (50) µm batches were used; the smallest is resolved by roughly four pixels and therefore probes the lower limit of the retrievable size range. ~~three sizes were chosen, 15 um, 30 um and 50 um~~. It detects all three sizes well, as shown in ~~(~~Figure 4~~)~~. All three batches were detected and sized to within two pixels of their certified means (Figure 4, left column): 18.5 µm for the 14.4 µm beads, 32.9 µm for the 29.5 µm beads and 55.9 µm for the 49.3 µm beads, corresponding to biases of +1.19, +0.99 and +1.91 px respectively. Although these correspond to relative errors ranging from 11 % to 29 %, the bias expressed in pixels is nearly constant and shows no systematic dependence on particle size. This is characteristic of a fixed edge-localization offset in the sizing algorithm rather than of an error in the magnification or in the reconstruction geometry, which would instead produce a constant relative error. The mean high-resolution bias of approximately +1.3 px sets the practical sizing accuracy of the system and, as expected, dominates the relative error budget at the smallest sizes.~~Both the 15 um and 30 um beads were measured within one pixel accuracy – at 18.5 um and 32.9 um respectively. The 50 um beads were still rather close at 55.9 um.~~

The high speed system has a shorter exposure time, which increases the reliable retrieval limit. Thus, the 42.3 (40) and 49.3 (50) µm batches were used instead, consistent with the intended application of the high-speed configuration to the larger, faster-falling drizzle mode rather than to the small cloud droplet mode. The 49.3 µm batch was measured with both cameras and therefore provides a direct comparison in which the target is physically identical, and only the imaging chain differs.

~~The dataset is unfortunately not very clean and a lot of aerosols from the air can air turbulence can be seen, as shown in the example holograms in Figure 4. The glass beads have to be transported into the sample volume, and the air turbulence from the carrier air flow was rather strong and can be seen in the holograms. This leads to a slight oversizing of the beads due to more intensity fluctuations of the background image, as particles are harder to find in these circumstances.~~

~~For the high speed camera, beads with diameters of 40 um and 50 um were chosen (Figure 4, right column).~~ While the 40 µm ~~um~~ were detected very close to the actual size (40.8 µm ~~um~~ from HOLODROPS), the 50 µm beads, by contrast, were retrieved at 62.6 µm, an overestimate of 13.3 µm or 27 %. Since the same bead batch was sized to 55.9 µm by the high-resolution system, and since the 42.3 µm beads measured with the same camera show no comparable bias, this discrepancy cannot be

attributed to the reference material or to a fixed instrumental offset. ~~50 um beads were measured larger (62.6 um)~~. Instead, we attribute it to the injection conditions: the heavier 50 µm beads required a stronger carrier flow to be entrained into the sample volume, thereby increasing both the interference aerosol loading and the inhomogeneity along the beam path. The same trend, though weaker, is present in the high-resolution data. The effect is amplified in the high-speed system because its shorter exposure time and larger pixels yield a lower signal-to-noise ratio per frame, so a given level of background fluctuation degrades fringe contrast and, hence, edge localization more severely.~~This discrepancy can be explained by the fact that the 50 um beads had much higher noise levels due to the air flow than the 40 um beads, similar to the oversizing of the HR system~~. We therefore interpret the 49.3 µm high-speed result as an upper bound on the sizing bias under unfavorable imaging conditions rather than as an intrinsic property of the instrument.

Table 2. Glass beads information with the retrieved mean diameters.

Camera	Certified D_{beads} (µm)	$D_{Retrieved}$ (µm)	Bias (µm)	Bias (%)
High resolution	14.4 ± 0.8	18.5	4.1	28.5
High resolution	29.5 ± 1.0	32.9	3.4	11.5
High resolution	49.3 ± 1.4	55.9	6.6	13.4
High speed	42.3 ± 1.1	40.8	−1.5	−3.5
High speed	49.3 ± 1.4	62.6	13.3	27

Formatted: Subscript
Formatted: Centered
Formatted Table
Formatted: Centered
Formatted: Centered
Formatted: Centered
Formatted: Centered
Formatted: Right
Formatted: Centered

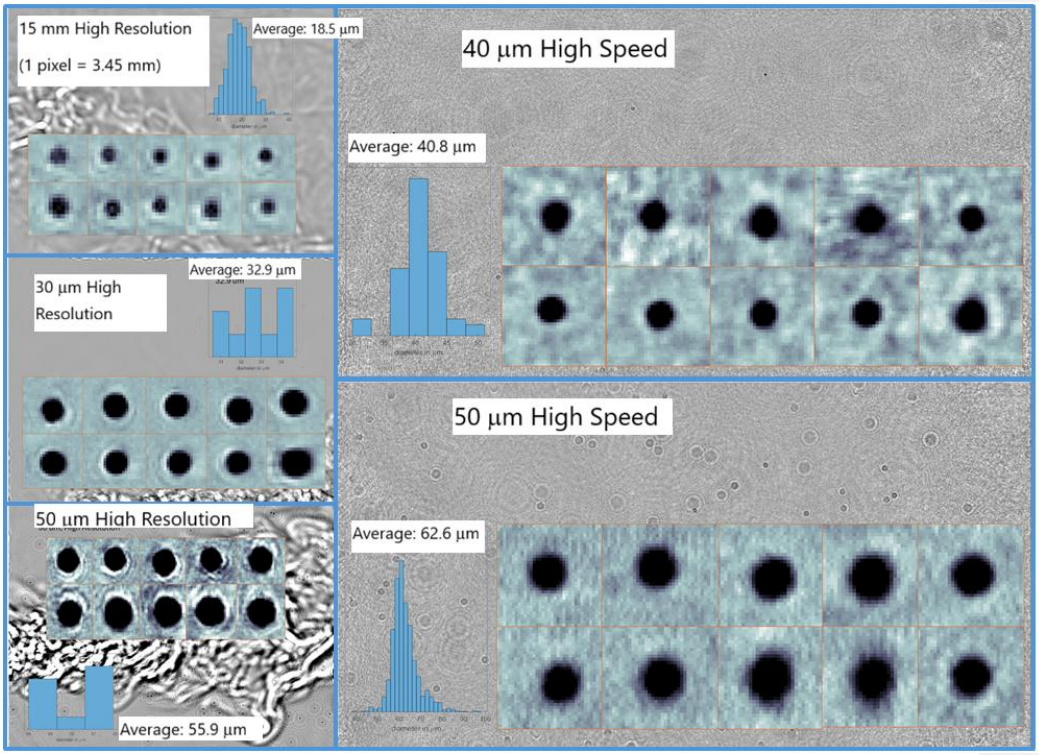


Figure 4: Results of glass bead tests with both systems: High resolution (left) and high speed (right) camera. Each panel shows a reconstructed plane of one of the holograms taken for this size (background), 10 examples of what beads looked like and the determined size distribution. The histogram plot x-axis is the diameter in µm and y-axis represents the probability density at each size bin.

Formatted: Font: Symbol

3.3 Outdoor drizzle measurements

Formatted: Heading 2

To test the instrument at realistic conditions, we deployed HOLODROPS at an instrument platform outside during a drizzle event on 13 March 2026 in Richland, WA, USA. The setup and results are shown in Figure 5; shown are the laser system, the camera system, and the sample volume. The sample distance between camera and laser system was 32.3 cm, leading to an effective sample volume of 106 cm^{3}~~^3~~. Unfortunately, the system was not able to be properly aligned, leading to the shading of parts of the hologram (large semi-circle in the righthand part of the hologram in Figure 5), which will necessitate some improvements of the setup. It reduced the sample volume by 12%, still giving a very large sample volume for this experiment.

The black covers shown in the setup were a necessary safety feature eliminating laser scattering, and while it will impact airflow and thus results, there are plans to improve laser safety and deployments to a location where these safeguards are not needed.

During the duration of the measurement was constant drizzle with varying intensity, shown in the time series in Figure 5. The average size of drizzle drops was 377 um, with a large spread. The holograms are great quality and the drops are well detected, with clear images obtained from reconstruction.

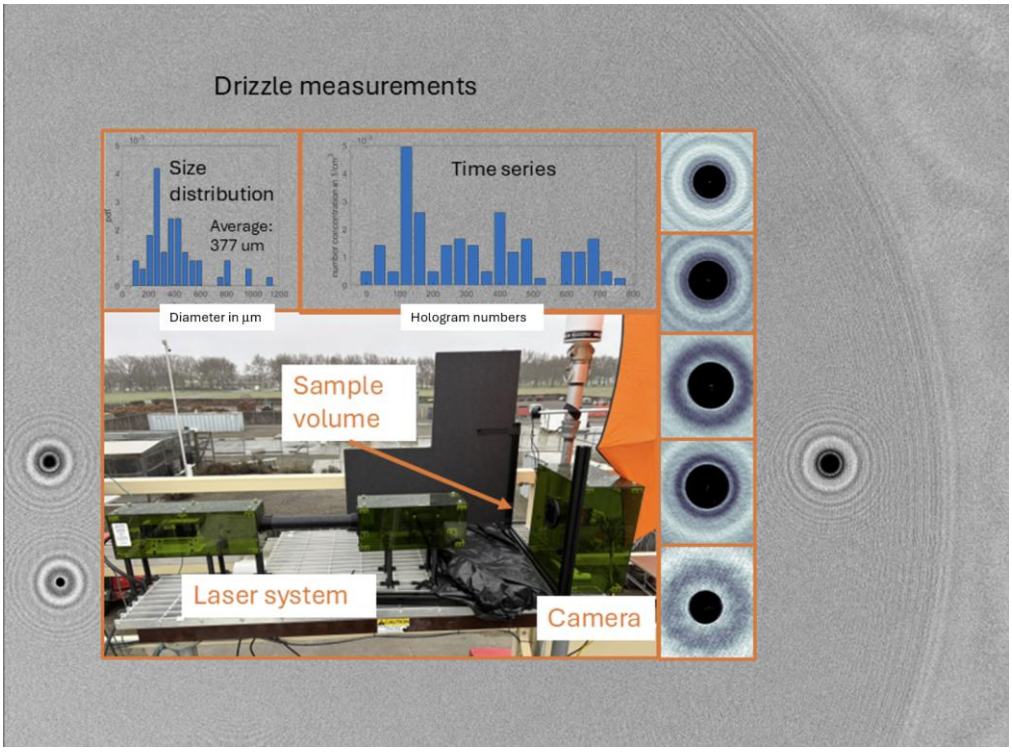


Figure 5: Results from outdoor drizzle measurements: Background shows an example of a hologram with three drizzle drops within the same frame; insert shows the size distribution and time series measured as well as the experimental setup and five examples of drizzle drops.

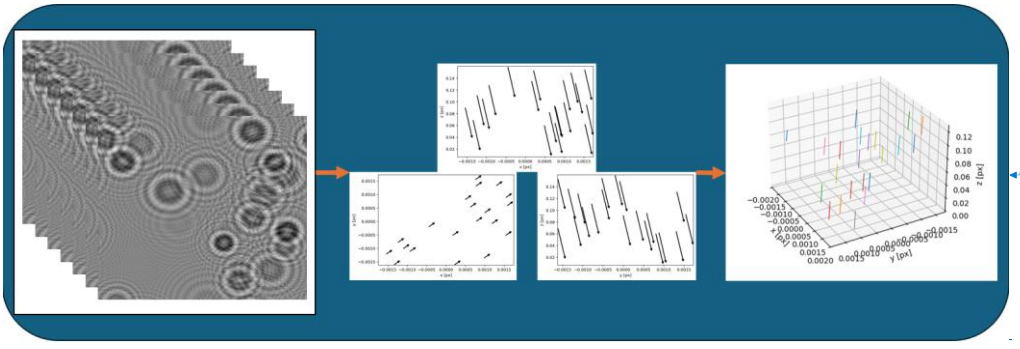
Overall, the outdoor deployment was a successful proof of concept, and HOLODROPS will be able to be used in both indoor and outdoor situations. For long-term outdoor operation, a few improvements will be made, such as temperature control of the electronics, waterproofing of the housing, better splash-resistance of the windows, and improved laser safety with less impact

on the sample volume air-flow. We also saw some movement of the components in wind, and therefore a sturdier, smaller enclosure of the laser setup will be designed. However, even without these future improvements the system works remarkably well with clean data.

3.4 Evaluation of Particle Tracking Capability of HOLODROPS-TRACK

With the use of the high-speed cameras for image and hologram captures ~~we can capture droplets lactation and sizes in in~~ , we can capture droplet locations and sizes in rapid succession. This creates the possibility of employing particle tracking software to infer additional information from the droplets such as individuals a combined particle velocities in a 3 D. This will require software that can link particles together between holograms and determining the vector velocities for further analysis. Now there is no particle tracking software specifically designed for droplet holograms, but there are many general articles tracking software's that could be valid candidates.

For this project, Holosuite is used to reconstruct particles~~create holograms~~ and determine the 3-dimensional positions of particles between frames and Trackpy was used to link the particles together to represent the same particle between frames. Along with information on the pixel sizes, and framerate of the camera, it allows to determine the velocity and direction of each individual particle. We used synthetic holograms for testing of the tracking calculations, and the results are shown in Figure 6. ~~Each simulated particle is set to move 3 mm in z, and 3 pixels, which translates~~ to 10.5 µm ~~um~~ in both x and y dimension, and the results reflect that. Each particle was found and moved by the prescribed distance.



S

Formatted: Heading 2

Formatted: Don't keep with next

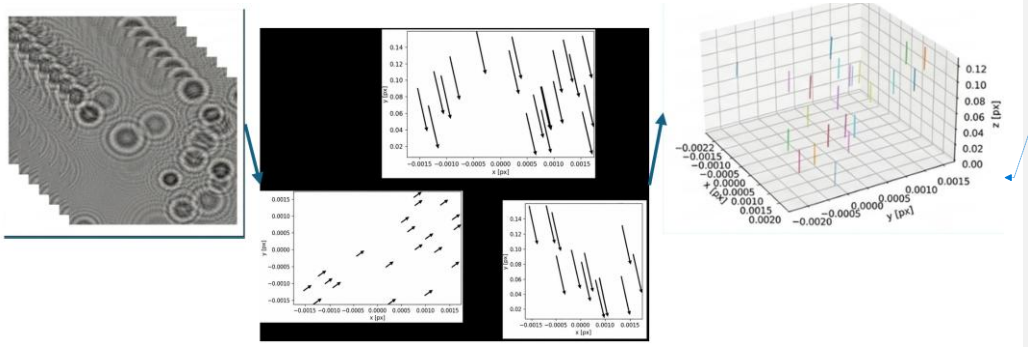


Figure 6: Results from particle tracking with synthetic holograms. Left: raw synthetic holograms. Center: Reconstructed particle movements in all three planes. Right: Particle tracks and movements in space.

The nebulizer flow was imaged using the high-speed HOLODROPS-TRACKs holographic system. Frames were recorded at 1397 frames per second with an exposure time of 15.99 µs. Raw holograms were reconstructed using the Holosuite software (Schlenczek, 2017) to obtain three-dimensional particle positions.

After reconstruction, particle trajectories were identified using the trackpy Python package (Allan et al., 2018; Crocker and Grier, 1996) Particle linking was performed with a search radius of 800 µm, and trajectories shorter than 20 frames were excluded from further analysis. ~~Particle velocities were then calculated by taking finite differences of the particle positions along each trajectory between consecutive frames.~~

The positional uncertainty in the holographically reconstructed particle data is approximately one pixel in both the x and y directions, where each pixel corresponds to 4.5 µm in the camera plane. The uncertainty in the z direction is governed by the axial reconstruction step size, which is about 100 µm. Random error in particle trajectory positions is estimated by fitting a polynomial to each identified track and evaluating the residual variance and covariance of the fitted coefficients (Janke and Michaelis, 2021). The positional residual standard deviation is calculated using $\sigma_p = \frac{\Sigma(p_j - \hat{p}_j)^2}{\sqrt{n-3}}$ with σ_p as the position uncertainty, p_j is the measured particle position, $\hat{p}$ is the fitted position, and n is the number of points in a track.

Velocity uncertainties are obtained by analytically differentiating the second-order polynomial fit to position as a function of time. Applying the chain rule yields a linear expression for velocity in terms of the polynomial coefficients. The Jacobian of this transformation propagates the positional uncertainties into the corresponding velocity components.

Formatted: Normal

A total of 392 particles were initially tracked, and trajectories containing fewer than four points were removed, leaving 157 usable tracks. Velocities were then evaluated at each time step from the differentiated polynomial fits. Table ~~1~~3 in the manuscript summarizes the RMS positional uncertainties and mean velocity uncertainties.

Table ~~1~~3: Mean uncertainty values for the positional and velocity components for the tracked particle.s

Component	Mean velocity (μm/s)	Mean Velocity uncertainty (μm /s)	RMS Position Residual (μm)
u/x	94.67	1.90	7.24
v/y	-61.19	1.42	7.31
w/z	-122.95	57.25	115.02

Figure 7 presents representative particle trajectories reconstructed from the holograms. Each color denotes a distinct particle track. The three-dimensional paths are shown alongside their two-dimensional projections onto the x–y and y–z planes. The left panel displays the y–z projection, while the right panel shows the x–y projection.

~~shows representative particle trajectories obtained from the holographic reconstruction. Each color corresponds to an individual particle track. The three-dimensional trajectories are shown together with their two-dimensional projections onto the x–y and y–z planes. The left panel of Figure 7 shows the y–z projection of the trajectories, while the right panel shows the x–y projection.~~

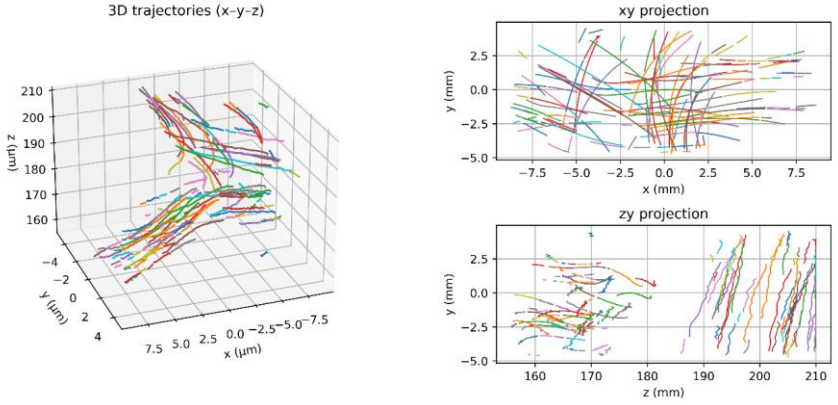


Figure 7: Left: Three-dimensional particle trajectories obtained from holographic reconstruction, along with their 2D projections. Right Top: x–y projection of the particle tracks. Each color represents a different particle. Left Bottom: z-y projection of the particle tracks.

Additional plots of RMS residuals illustrate the uncertainty distribution for each spatial component in Figure 8. As expected, the x and y components exhibit smaller uncertainties because they are directly tied to pixel resolution, while the z component shows significantly larger variability due to its dependence on the axial reconstruction step. The residual distributions were found to be:

•x-position:7.24 ± 13.58 µm

•y-position:7.31 ± 15.68 µm

• z-position: 115.02 ± 53.10 µm

These results confirm that lateral positional uncertainties are much tighter than axial uncertainties, consistent with the characteristics of digital in-line holography.

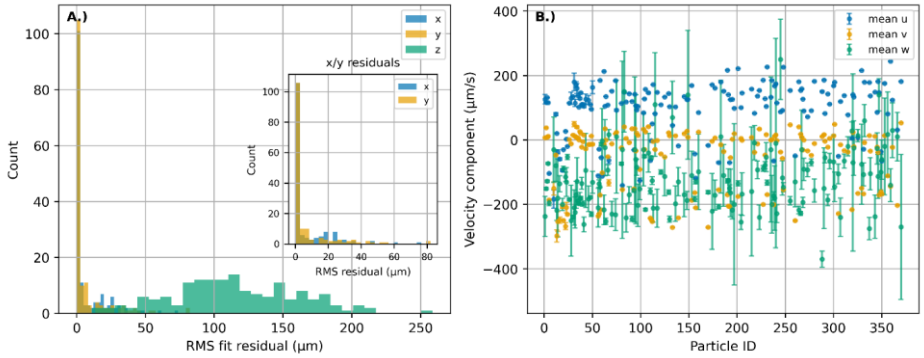


Figure 8: A.) displays the residual distributions for the particle-track positions obtained from the polynomial fits, with the inset highlighting the x- and y-component residuals. Panel B shows the velocity components and their associated uncertainties for each particle track. In total, 392 particle tracks were initially identified. After removing tracks shorter than 4 points, 157 complete particle trajectories remained for analysis.

3.5 Evaluation of the Tracking Capability of ePIV

To assess the performance and uncertainty of the ePIV system, we generated synthetic particle-image data with known displacement fields. This provides a controlled environment for quantifying position and velocity errors and follows established best practices for PIV uncertainty analysis (Sciacchitano, 2019). The goal is not to establish the absolute measurement uncertainty but rather to determine a practical upper bound for uncertainty under conditions matched to our experiment.

Formatted: Keep with next

Formatted: Heading 2

3.5.1 Synthetic Data Generation and Experimental Matching

Formatted: Heading 3

We first established frame-based experimental statistics to ensure the simulations closely matched real measurements. Particle density was calculated using a connected-component algorithm, allowing estimation of the number of particles per interrogation window. Additional statistics including particle diameter, intensity distribution, and active pixel area were derived from autocorrelation analysis of experimental frames. These metrics provide realistic seeding conditions and ensure similar signal-to-noise characteristics between synthetic and experimental data. This analysis was conducted for different time intervals from 1.0 ms to 10 ms, and showed comparable statistics across frames.

To simulate realistic PIV input, SynthPix was used to generate uniform displacement fields ranging from 1 to 9.5 px at randomized orientations, with 20 realizations per displacement magnitude (**Terpin et al., 2026**). The frame size (256×256) is sufficient for capturing statistical behavior without requiring full-frame simulations. Each synthetic pair was padded to accommodate edge displacements, ensuring physically valid particle origins.

A median filter was used to suppress isolated sensor noise in experimental data; however, because synthetic noise was not simulated, filtering was omitted in the synthetic pipeline.

The statistical parameters used to align the simulations with the experimental data included a seeding density of 1–3 particles per pixel, particle diameters ranging from 1.6 to 1.87 pixels with a variance of 0.3 pixels, signal-to-noise ratios between 1 and 1.2, total displacement magnitudes from 1 to 9.5 pixels, and 20 simulation realizations.

44

3.5.2 Velocity Field Computation and Uncertainty Estimation

Formatted: Heading 3

Pseudo-frames were constructed at 1 ms intervals to align with the temporal resolution used during ePIV acquisition. These frames were processed using openPIV, employing cross-correlation within 16-pixel interrogation windows and a 19-pixel search area. Prior to processing, median filtering was applied to remove pixel-level noise inherent to the event camera.

Velocity fields were calculated for each frame pair, and a time-averaged velocity field was formed by averaging all instantaneous velocity components across the full acquisition period. Though instantaneous velocities can be high, variations in droplet appearance within the light sheet lead to relatively small mean values.

Uncertainty quantification follows the established approach of comparing known synthetic displacements to measured correlation-based displacements. By matching simulation parameters—particle size, seeding density, intensity, and signal-to-noise ratios—to experimental statistics, the resulting displacement-error curves provide a consistent upper bound on measurement uncertainty (Sciacchitano, 2019).

Figure 9 shows the error for displacement vectors. The error is bined with respect to the peak-to-peak SNR to determine a corresponds to the experiment. The dispalcment error average values was fround to be between 4.7

pixels to 1.7 for a peak-to-peak SNR of 1-1.38. The vectors are transvered in random directions, so the errror for the x and y direction follow the same profile, and magnitude.

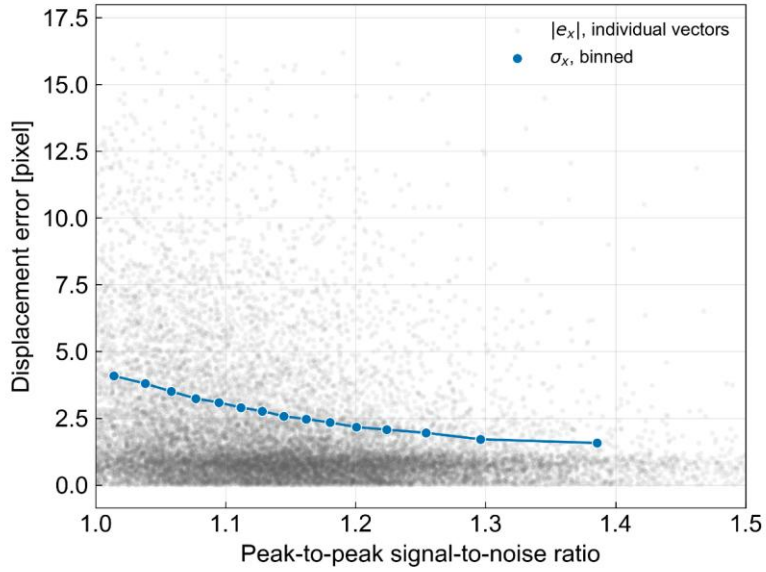


Figure 9: After calculating the error in displacement of simulated particles. The displacement error is binned with respect to the peak-to-peak SNR ratio. As the SNR increase the displacement error decreases providing an estimate for the particle displacement uncertainty from the determined SNR ratios.

After determining the displacement error, the error in the calculated velocity can be determiend from $\sigma_v = \frac{\sigma_{px} S}{\Delta t}$ with σ_v as the velocity uncertainty, σ_{px} as the displacement uncertainty, S as the scaling factor, and Δt as the time interval. For our experimeint, at 0.01 ms and a scaling factor of 0.033mm/px makes the velocity uncertainty $\sigma_v = 3.3\sigma_{px}$ with unites of $[\frac{mm}{s}]$.

~~After constructing pseudo-frames at 10-millisecond intervals, openPIV (Shirinzad et al., 2023) was employed to analyze the frames and calculate the velocity field. Before processing, a median filter was applied to the pseudo-frames to eliminate pixel noise generated by the event camera. The extended search method was utilized to calculate cross-correlation between frames, with an interrogation window size set to 16 pixels and a search area of 19 pixels.~~

~~Velocity fields were determined for each pair of consecutive frames. The average velocity field was obtained by summing the vector field components across all frames and dividing by the total number of frames.~~

Formatted: Keep with next

3.5.3 Orientation-Dependent Measurement Strategy

Formatted: Heading 3

Since ePIV captures only two velocity components within a thin laser sheet, measurements were collected from two orientations to approximate broader flow characteristics:

1. Side-view: droplets traverse perpendicular to the laser-sheet propagation.
2. Front-view: droplets move within the plane of the sheet.

Each experiment used a 10-second acquisition period with 1.0-ms separations between frames. While many frames contain few particles, this duration is sufficient for resolving persistent background flow patterns and intermittent turbulent structures. SEQ Figure * ARABIC ~~Figure 10~~ shows the fluid flow of the particles captured using the event camera. Positive (white) events indicate increases in pixel intensity—corresponding to current droplet locations—while negative (blue) events denote intensity decreases, tracing particle histories. These signatures provide intuitive visualization of flow direction.

~~For the ePIV (Event Particle Image Velocimetry) measurements, a laser light sheet was positioned 50 mm from the front of the camera lens. Measurements were performed with the nebulizer located (i) directly to the side of the light sheet and (ii) directly in front of it. The flow field was recorded for a duration of 10 s, and velocity fields were computed between successive image pairs with a time separation of 10 ms. The resulting instantaneous velocity fields were then averaged over the full 10 s acquisition period. Given the efficient read out, and sparse data representation, several minutes of data was recorded, but 10 seconds was sufficient to capture the flow field dynamics. Examples of captured particle flows are shown in Figure 8.~~

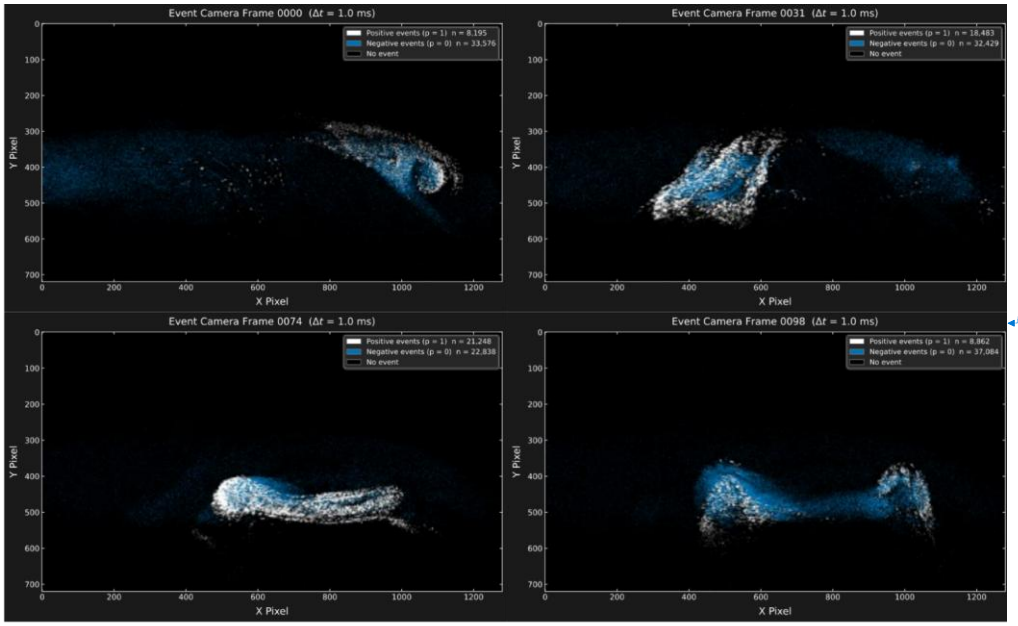


Figure 10: Captured fluid flows using an event camera: The event data was collected over a 1-millisecond time interval. Positive events, represented by white markings, signify areas where light intensity increases, while negative events, marked in blue, denote regions where light intensity decreases. These visualizations can be interpreted as follows: the white markings highlight the current locations of water droplets, whereas the blue markings indicate past positions of the droplets as they moved.

3.5.4 Spatial Calibration and Velocity Scaling

Spatial calibration was achieved using a checkerboard target placed 50 mm from the optical system. The resulting scale factor of 31.6 pixels/mm was applied to convert all measured velocities from pixels/s to physical units (mm/s). Instantaneous velocities occasionally reached 300 mm/s, though time-averaged values were closer to 20 mm/s. The full distribution of measured speeds is shown in Figure 11. ~~[AMT-Holodrops-v2 | Word]~~

3.5.5 Summary of ePIV Tracking Performance

Overall, the ePIV system effectively captures fluid motion using event-camera data. Synthetic-data matching ensures reliable uncertainty bounds, and dual-orientation experiments improve interpretation of complex flow structures. While ePIV measures

Formatted: Keep with next

Formatted: Heading 3, Don't keep with next

Formatted: Heading 3, Don't keep with next

only in-plane velocities, it provides rapid, low-latency flow information across many particles, making it strongly complementary to the holographic particle-tracking system, which resolves full 3D trajectories over shorter intervals.

~~**Figure 8: Captured fluid flows using an event camera: The event data was collected over a 2-millisecond time interval. Positive events, represented by white markings, signify areas where light intensity increases, while negative events, marked in blue, denote regions where light intensity decreases. These visualizations can be interpreted as follows: the white markings highlight the current locations of water droplets, whereas the blue markings indicate past positions of the droplets as they moved.**~~

~~To determine the spatial calibration, a checkerboard calibration target was placed 50 mm in front of the optical system. The known square size was used to compute the pixel-to-distance conversion factor. At this distance, the scaling factor was found to be 31.6 pixels/mm. This calibration was used to convert the measured velocities from pixels/s to mm/s.~~

~~The time-averaged velocity fields are shown in Figure 9. Both the side-view and front-view configurations reveal a persistent background flow in the room, with a dominant velocity component in the x-direction. During the 10 s acquisition period, many frames can be empty, or only show a few particles present within the light sheet. For this reason, the average velocity field~~

appears quite small even though instantaneous velocities can be quite high. On average the particle velocities are closer to 20 mm/s, but in a few cases can be as large as 300 mm/s. The overall distribution of recorded speeds is shown in Figure 10.

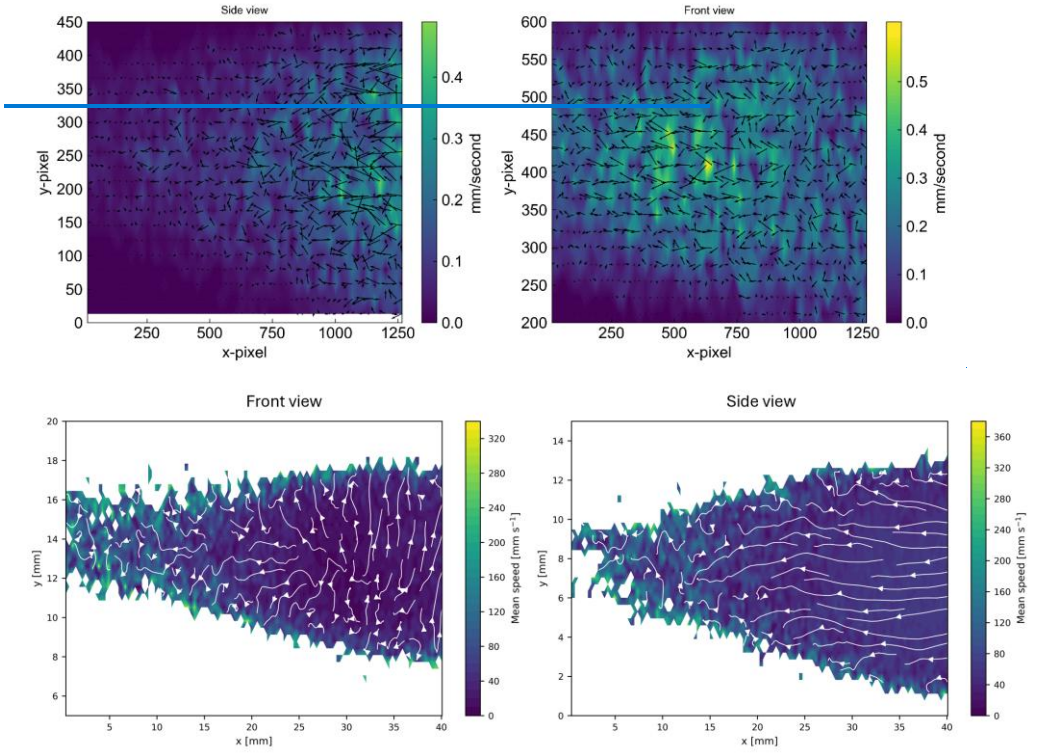


Figure 11119: Time-averaged velocity fields measured using the ePIV system. Left: side-view measurement of the nebulizer relative to the light sheet. Right: front-view measurement. Arrows indicate the direction and magnitude of the measured velocity.

(Sciacchitano, 2019; Terpin et al., 2026; Hu et al., 2021)

3.6 HOLODROPS-TRACK and ePIV Performance Comparison

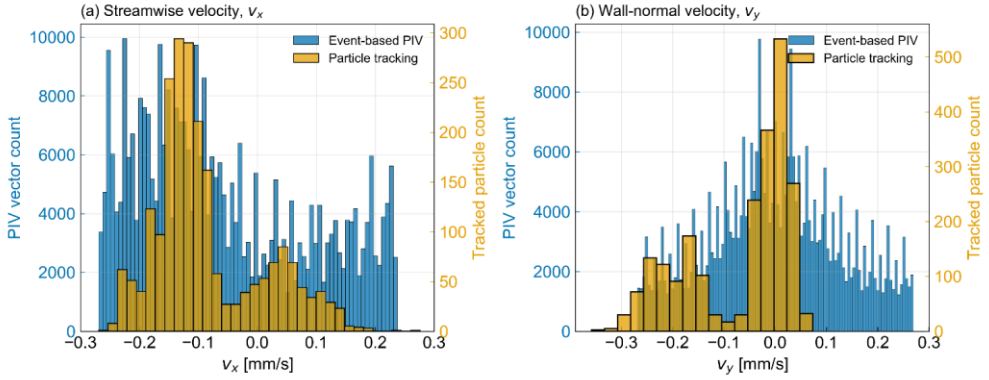
Formatted: Heading 2

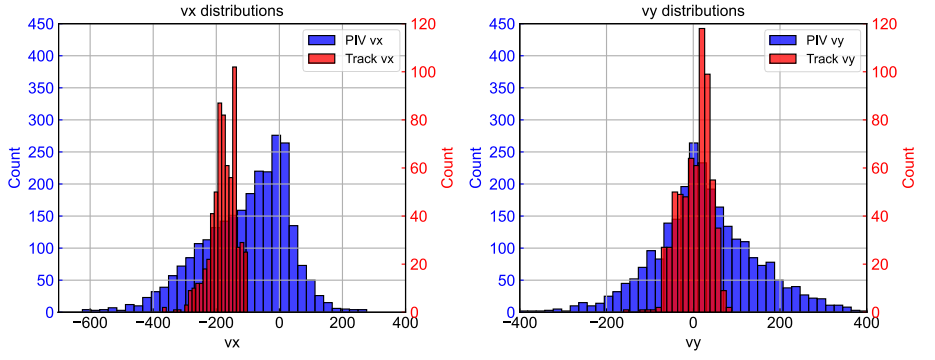
The distributions of particle velocities are shown in ~~Figure 10~~Figure 12. Both the ePIV measurements and the particle tracking results exhibit a pronounced mean flow in the negative x-direction. The distributions of the y-velocity components are approximately centered around zero for both methods, indicating no significant net motion in the y-direction. The laboratory environment has an HVec system which continuously filtered air. This system creates a steady draft in the laboratory, and causes the particles to gradually flow in the -x-direction which was observed with both experiments.

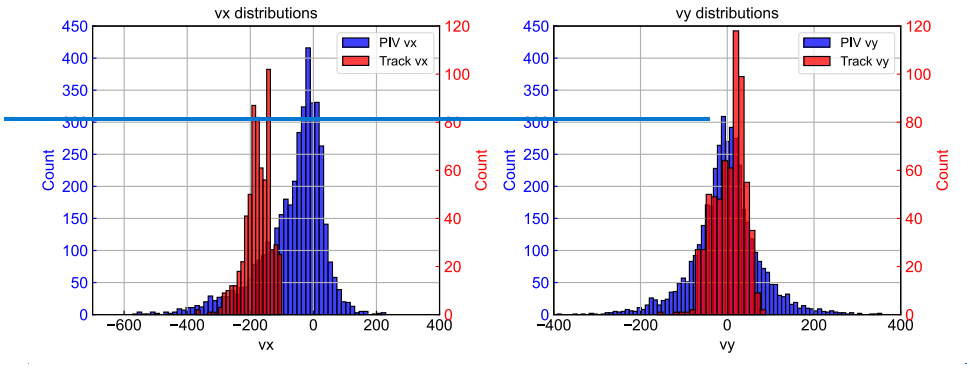
In the ePIV configuration, only a thin slice of the flow intersecting the light sheet is captured, so the measured velocities represent a cross-section of the full three-dimensional motion. In contrast, the HOLODROPS-HS holographic system resolves the full 3D position of individual particles over time, enabling direct estimation of all three velocity components, including the z-component. From the reconstructed z-positions, a net flow in the negative z-direction is observed. However, because the axial (z) position is inferred from holographic reconstruction, its spatial resolution is lower than that of the x and y coordinates, leading to comparatively higher uncertainty in the z-velocity component.

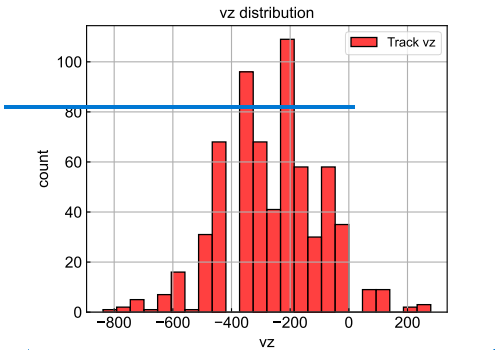
Additionally, the ePIV measurements cover a longer time interval and a larger number of particles passing through the light sheet compared to the holographic particle tracking, which is limited to a shorter acquisition duration. As a result, the ePIV

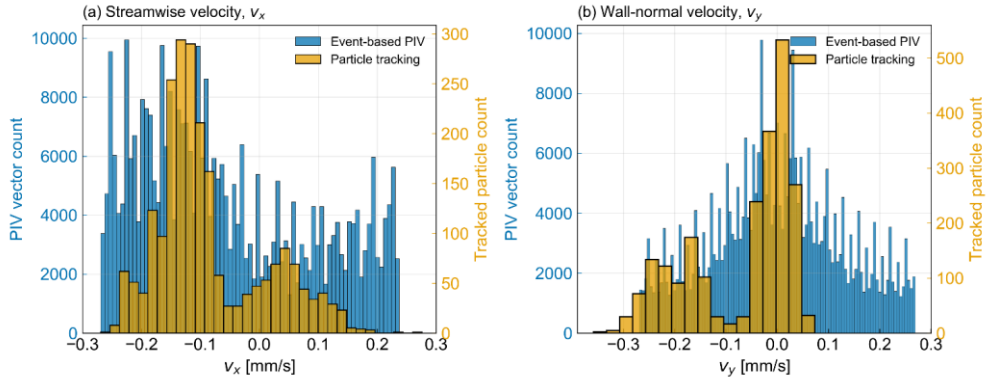
system is more sensitive to intermittent and turbulent fluctuations over extended timescales, whereas the holographic tracking provides detailed, fully three-dimensional trajectories over shorter periods.






vx distributions
PIV vx
Track vx
Count
Count
vx
vy distributions
PIV vy
Track vy
Count
Count
vy


vz distribution
Track vz
count
vz


(a) Streamwise velocity, v_x
Event-based PIV
Particle tracking
PIV vector count
Tracked particle count
v_x [mm/s]
(b) Wall-normal velocity, v_y
v_y [mm/s]

645

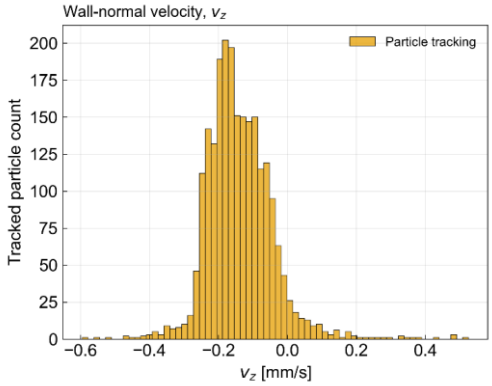


Figure 121210: Comparison of velocity distributions measured by holographic particle tracking and the ePIV system. Top: front-view configuration, showing x-velocity (left) and y-velocity (right) distributions for both methods. Bottom: side-view ePIV measurements of the nebulizer flow field.

Formatted: Caption

In summary, this study highlights the effectiveness of event cameras and inline holographic imaging for analyzing fluid flows and particle scattering dynamics. The event camera's low latency and inherent ability to detect pixel intensity changes enabled the real-time visualization of velocity fields and particle distribution.

4. Conclusions and Future Work

Three new cloud measurement systems were developed, HOLODROPS, HOLODROPS-TRACK and ePIV, and all were successfully characterized. The holographic systems are for long-term measurements of cloud droplet size distributions (HOLODROPS) and for particle tracking at short intervals (HOLODROPS-TRACK). We showed successful measuring of droplets larger than 8.8 µm ~~um~~ in diameter, both in a laboratory setting and in a drizzle case outside. HOLODROPS-TRACK identified 3-dimensional tracks of the particles moving through the sample volume, which will enable direct studies of atmospheric turbulence as well as the detection of collision-coalescence as it happens. HOLODROPS is designed to capture the entire size distribution range of cloud droplets up to drizzle and ice crystals, without the need of several instruments with narrow size ranges. HOLODROPS can run outside in drizzle conditions, however, for longer deployments the system still needs to be thoroughly weatherproofed. This is the next step for HOLODROPS, with the addition of waterproof housing. Furthermore, in the future HOLODROPS will be run in extreme hot and cold conditions, such as mountain-tops in winter as

well as the heat of summer, so heating and cooling elements for the critical electronic components (laser, camera and data acquisition) will be necessary.

Initial data processing for HOLODROPS and HOLODROPS-TRACK is currently done with Holosuite software, and very time consuming and computationally expensive. Future work would therefore focus on speeding up the processing time, which would enable faster data accessibility, and improving the particle detection, leading to better data quality.

The ePIV is an event-camera based particle imaging velocimetry system, which perfectly complements the holographic measurements. It measures the flow directly and can be viewed in real time to inform ongoing measurements. Due to the dynamic readout the ePIV system produces lower data volume and processing time, which is a limitation to HOLODROPS-TRACK system. ePIV can operate continuous for long periods of time; ePIV can inform users about cloud conditions much faster than holography, and can inform when the conditions would be ideal to collect data with HOLODROPS-TRACK for finer detail. Both HOLODROPS-TRACK and ePIV are able to capture comparable fluid flows. Though the HOLODROPS-TRACK provides more detailed information for the individual particles tracked. In comparison, ePIV is not limited to individual particles and can gather information on a larger sample size. Future work will extend ePIV to measure 3 dimensional fluid flows.

Acknowledgements

This research is part of the Drizzle Representation via Enclosed Atmosphere Measurements and Modeling (DREAM2) Initiative at Pacific Northwest National Laboratory (PNNL). It was conducted under the Laboratory Directed Research and Development Program at PNNL, a multi-program national laboratory operated by Battelle for the U.S. Department of Energy under Contract DE-AC05-76RL01830.

References

Lecture 3: https://www.gfdl.noaa.gov/wp-content/uploads/files/user_files/pag/lecture2008/lecture3.pdf, last

Allan, D. B., Caswell, T., Keim, N. C., and van der Wel, C.: trackpy: Trackpy v0.7, online [code], 2018.

Baumgardner, D., Brenguier, J., Bucholtz, A., Coe, H., DeMott, P., Garrett, T., Gayet, J., Hermann, M., Heymsfield, A., and Korolev, A.: Airborne instruments to measure atmospheric aerosol particles, clouds and radiation: A cook's tour of mature and emerging technology, Atmospheric Research, 102, 10–29, 2011.

Beck, A., Henneberger, J., Schöpfer, S., Fugal, J., and Lohmann, U.: HoloGondel: in situ cloud observations on a cable car in the Swiss Alps using a holographic imager, Atmospheric Measurement Techniques, 10, 459–476, 10.5194/amt-10-459-2017, 2017.

Beresh, S. J., Miller, N. E., and Smith, B.: Practical challenges in the calculation of turbulent viscosity from PIV data, 2018 Aerodynamic Measurement Technology and Ground Testing Conference, 2987,

Crocker, J. C. and Grier, D. G.: Methods of digital video microscopy for colloidal studies, Journal of colloid and interface science, 179, 298–310, 1996.

Fugal, J. P. and Shaw, R. A.: Cloud particle size distributions measured with an airborne digital in-line holographic instrument, Atmospheric Measurement Techniques Discussions, 2, 659–688, 10.5194/amtd-2-659-2009, 2009.

Fugal, J. P., Shaw, R. A., Saw, E. W., and Sergeyev, A. V.: Airborne digital holographic system for cloud particle measurements, Applied optics, 43, 5987–5995, 10.1364/AO.43.005987, 2004.

Gallego, G., Delbrück, T., Orchard, G., Bartolozzi, C., Taba, B., Censi, A., Leutenegger, S., Davison, A. J., Conradt, J., and Daniilidis, K.: Event-based vision: A survey, IEEE transactions on pattern analysis and machine intelligence, 44, 154–180, 2020.

Henneberger, J., Fugal, J. P., Stetzer, O., and Lohmann, U.: HOLIMO II: a digital holographic instrument for ground-based in situ observations of microphysical properties of mixed-phase clouds, Atmospheric Measurement Techniques, 6, 2975–2987, 10.5194/amt-6-2975-2013, 2013.

Hu, Y., Liu, S.-C., and Delbruck, T.: v2e: From video frames to realistic DVS events, 2021 IEEE/CVF Conference on Computer Vision and Pattern Recognition Workshops (CVPRW), 1312–1321,

Janke, T. and Michaelis, D.: Uncertainty quantification for PTV/LPT data and adaptive track filtering, 14th international symposium on particle image velocimetry,

Kaikkonen, V. A., Molkoselkä, E. O., and Mäkynen, A. J.: A rotating holographic imager for stationary cloud droplet and ice crystal measurements, Optical Review, 27, 205–216, 10.1007/s10043-020-00583-y, 2020.

Lance, S., Brock, C. A., Rogers, D., and Gordon, J. A.: Water droplet calibration of the Cloud Droplet Probe (CDP) and in-flight performance in liquid, ice and mixed-phase clouds during ARCPAC, Atmospheric Measurement Techniques, 3, 1683–1706, 10.5194/amt-3-1683-2010, 2010.

LU, C.-S., LIU, Y.-G., NIU, S.-J., and XUE, Y.-Q.: Broadening of cloud droplet size distributions and warm rain initiation associated with turbulence: An overview, Atmospheric and Oceanic Science Letters, 11, 123–135, 2018.

Lu, J., Fugal, J. P., Nordsiek, H., Saw, E. W., Shaw, R. A., and Yang, W.: Lagrangian particle tracking in three dimensions via single-camera in-line digital holography, New Journal of Physics, 10, 125013, 2008.

Meng, H., Anderson, W., Hussain, F., and Liu, D. D.: Intrinsic speckle noise in in-line particle holography, Journal of the Optical Society of America A, 10, 2046–2058, 1993.

Nelli, N., Francis, D., Abida, R., Fonseca, R., Masson, O., and Bosc, E.: In-situ measurements of fog microphysics: Visibility parameterization and estimation of fog droplet sedimentation velocity, Atmospheric Research, 309, 107570, 2024.

Pinsky, M. and Khain, A. P.: Fine Structure of Cloud Droplet Concentration as Seen from the Fast-FSSP Measurements. Part I: Method of Analysis and Preliminary Results, Journal of Applied Meteorology, 40, 1515–1537, 10.1175/1520-0450(2001)040<1515:FSOCDC>2.0.CO;2, 2001.

Podzimek, J.: Droplet concentration and size distribution in haze and fog, Studia Geophysica et Geodaetica, 41, 277–296, 1997.

Ramelli, F., Beck, A., Henneberger, J., and Lohmann, U.: Using a holographic imager on a tethered balloon system for microphysical observations of boundary layer clouds, Atmospheric Measurement Techniques, 13, 925–939, 2020.

Royer, H.: An application of high-speed microholography: the mertology of fogs, Nouvelle Revue d'Optique, 5, 87–93, 1974.

Schlenczek, O.: Airborne and ground-based holographic measurement of hydrometeors in liquid-phase, mixed-phase and ice clouds, 2017.

Sciacchitano, A.: Uncertainty quantification in particle image velocimetry, Measurement Science and Technology, 30, 092001, 2019.

Shirinzad, A., Jaber, K., Xu, K., and Sullivan, P. E.: An enhanced python-based open-source particle image velocimetry software for use with central processing units, Fluids, 8, 285, 2023.

Spuler, S. M. and Fugal, J. P.: Design of an in-line, digital holographic imaging system for airborne measurement of clouds, Applied optics, 50, 1405–1412, 10.1364/AO.50.001405, 2011.

Strapp, J. W., Oldenburg, J., Ide, R., Lilie, L., Bacic, S., Vukovic, Z., Oleskiw, M., Miller, D., Emery, E., and Leone, G.: Wind tunnel measurements of the response of hot-wire liquid water content instruments to large droplets, Journal of Atmospheric and Oceanic Technology, 20, 791–806, 10.1175/1520-0426(2003)020<0791:WTMOTR>2.0.CO;2, 2003.

Tamrin, K. F. and Rahmatullah, B.: A review on noise suppression and aberration compensation in holographic particle image velocimetry, Cogent Physics, 3, 1142819, 2016.

Terpin, A., Bonomi, A., Banelli, F., and D'Andrea, R.: SynthPix: A lightspeed PIV image generator, SoftwareX, 34, 102642, 2026.

Thiede, B., Nordsiek, F., Kim, Y., Bodenschatz, E., and Bagheri, G.: HoloTrack: In-Situ Holographic Particle Tracking of Cloud Droplets, 10.5194/egusphere-2025-1774, 2025a.

Thiede, B., Nordsiek, F., Kim, Y., Bodenschatz, E., and Bagheri, G.: HoloTrack: in-situ holographic particle tracking velocimetry of cloud droplets, Atmospheric Measurement Techniques, 18, 5999–6019, 10.5194/amt-18-5999-2025, 2025b.

Thiede, B., Schlenczek, O., Stieger, K., Ecker, A., Bodenschatz, E., and Bagheri, G.: In-line holographic droplet imaging: accelerated classification with convolutional neural networks and quantitative experimental validation, Atmospheric Measurement Techniques, 18, 6291–6314, 10.5194/amt-18-6291-2025, 2025c.

Tiitta, P., Leskinen, A., Kaikkonen, V. A., Molkoselkä, E. O., Mäkynen, A. J., Joutsensaari, J., Calderon, S., Romakkaniemi, S., and Komppula, M.: Intercomparison of holographic imaging and single-particle forward light scattering in situ measurements of liquid clouds in changing atmospheric conditions, Atmospheric Measurement Techniques, 15, 2993–3009, 10.5194/amt-15-2993-2022, 2022.

Willert, C. E. and Gharib, M.: Digital particle image velocimetry, Experiments in fluids, 10, 181–193, 1991.

Willert, C. E. and Klinner, J.: Event-based imaging velocimetry: an assessment of event-based cameras for the measurement of fluid flows, Experiments in Fluids, 63, 101, 2022.

Supplemental Material. **Particle attenuation and holographic quality.**

For HOLODROPS and HOLODROPS-TRACK to work effectively both systems need to be able to capture an intense image and have good holographic quality. Light attenuation and hologram quality are dependent on the particle size, particle density, and thickness which particles are being imaged. First Mie theory is used to estimated light attenuation that could be caused by using beer-lambert law. Then the shadow parameter is calculated to determine the expected hologram quality.

For inline holographic imaging, water particles are expected to attenuate the laser beam and cause multiple interferences. The attenuation effect of the particles can be analyzed using Mie theory, whereas the interference they produce will generate speckles in the inline imaging. To estimate holographic degradation caused by such interferences, Royer criteria can be employed (Royer, 1974; Tamrin and Rahmatullah, 2016)~~(citation needed).~~

Mie theory describes the scattering behavior of spherical particles when the particle size is comparable to the wavelength of light, making it a suitable model for analyzing the behavior of water droplets in this study. Assuming a distribution of water particles, their scattering coefficients can be calculated using the *miepython* package in Python. The size of water droplets can vary depending on environmental conditions, and their interaction with laser beams also depends on the droplet size. For this experiment, a 405 nm laser is used to illuminate the particles, making scattering within this wavelength range the primary focus.

Mie theory is particularly suitable for scenarios where the wavelength of light is comparable to the size of the particles causing scattering. In this experiment, the 405 nm laser wavelength, coupled with water particles having a minimum diameter of 5 µm, results in a relatively constant scattering efficiency as shown in Figure S1. Additionally, water droplets are well-known for exhibiting strong forward scattering behavior.

The scattering, absorption, and extinction coefficients can be determined using the following equations:

$$\epsilon_{sc} = N\left(\frac{\pi D^2}{4}\right)Q_{sc} \quad (1)$$

$$\epsilon_{abs} = N\left(\frac{\pi D^2}{4}\right)Q_{abs} \quad (2)$$

$$\epsilon_{ext} = N\left(\frac{\pi D^2}{4}\right)Q_{ext} \quad (3)$$

Here, N represents the number concentration of particles ((particles/cm^3)), D is the particle diameter, and Q_x denotes the efficiency factors for scattering Q_{sc}, absorption Q_{abs}, and extinction Q_{ext}. The efficiency factors Q_x can be calculated for each particle in the distribution using the *miepython* package in Python at a wavelength of 405 nm .

To determine inline attenuation, the Beer-Lambert law is applied, assuming the single scattering approximation ((Noaa), 2008). Using the extinction coefficient, the attenuation of laser light intensity is calculated as:

$$I(z) = I_0 e^{-\epsilon_{ext} z} \quad (4)$$

The attenuation behavior was modeled for various particle concentrations and propagation distances. The results are illustrated in Figure S1. Two different particle distribution are considered. The first case assumes the mean particle distribution is close to the wavelength of the laser light at $0.5\ \mu m$. Then in the second case, with a mean $15\ \mu m$ which is consistent with the size of fog (Podzimek, 1997; Nelli et al., 2024). For an extreme case of 5000 particles per cubic centimeter ((particles/cm^3)),

laser light remains visible over a distance of up to 500 cm. This demonstrates the suitability of inline holographic imaging for environments with high particle densities

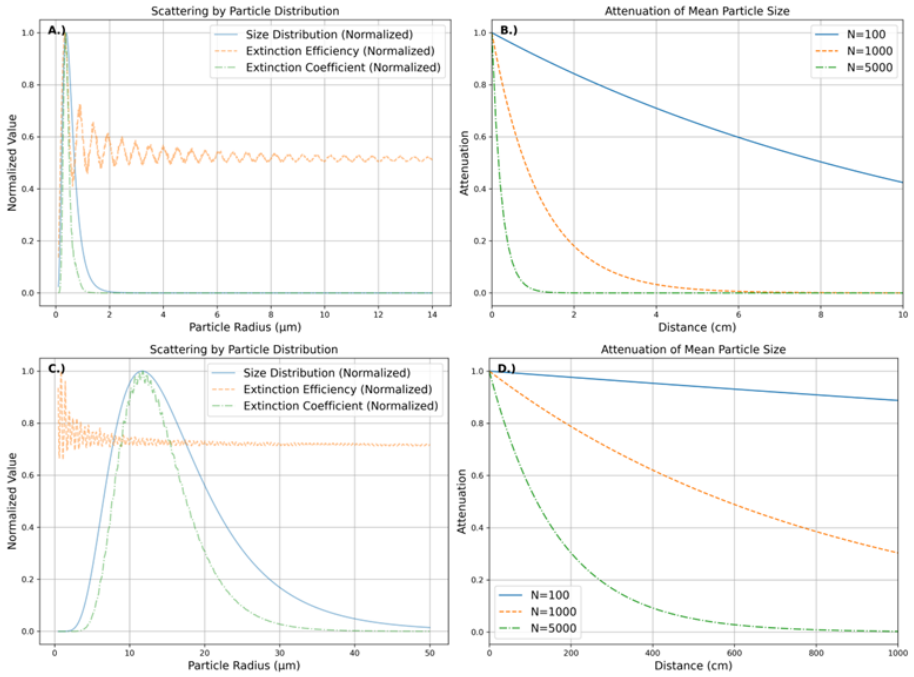


Figure S1: A.) A particle size distribution with the mean value is close to the wavelength of light at 05 μm. B.) attenuation of light for different number concentration of water droplets(number/um^3) over 10 cm for a particle distribution in panel A.). C.) A particle distribution with a mean size of 15 μm which is consistent with the size of fog. D) attenuation of light for different number concentration of water droplets(number/um^3) over 1000 cm for a particle distribution in panel D.).

In inline holography, the presence of water droplets acts as individual scatterers, contributing to speckle noise in the captured hologram. The quality of the hologram after passing through a distribution of particles can be characterized by the shadow

density parameter, also known as the Royer criterion, given by the equation:

$$S = N(\pi D_{mean}^2)Z \quad (5)$$

Here, N represents the particle concentration ((particles/cm$^{3\wedge\sout{3}}$)), D_{mean} is the mean particle diameter, and Z is the propagation distance (Meng et al., 1993).

As described in Meng et al. (Meng et al., 1993), the value of the shadow density parameter determines the quality of the resulting hologram:

- (S < 0.01): High-quality hologram.
- (0.01 <S ≤ 0.1): Marginal hologram.
- (S > 0.1): Poor-quality hologram.

The calculated results of the shadow density parameters for various experimental configurations are presented in Figure S2, demonstrating the relationship between particle concentration, mean particle size, and imaging distance on hologram quality.

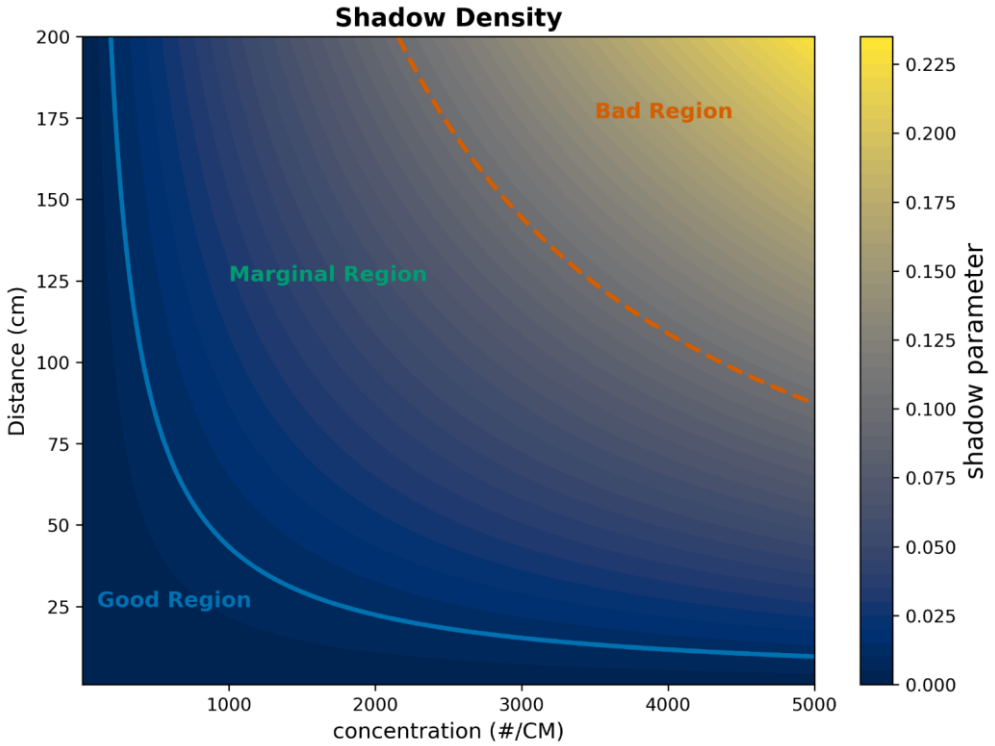


Figure S2 shadow parameters for holographic quality in terms of concentration and distance. The good, marginal and bad regions are separated by a line defining the respected value.

In conclusion, particle scattering is expected to have little effect on the light attenuation since the particle size with the most effective particle size is well below the resolution limit of the system. In addition, both systems should be able to collect holograms with particle densities of less than 1000/cm^3 and up to 1 meter optical depth.

To capture the varying turbulence flows the openPIV method outline in 2.2 ePIV prototype was ran for different time intervals. The laboratory had a steady breeze that would cause particles to steadily flow in the -x plane in the ePIV field of view. To draw a fair comparison the time duration was capture consistently at over 10 seconds total. The effect of keeping the time interval shorter shows more varied and turbulent flows throughout the measurements. This also results in more steady mean flows as shown in Figure S3 which shows the velocity fields for 1.0 ms, 5.0 ms, 10.0 ms, and 15.0 ms time intervals for the analysis process. As the time intervals decrease the mean flow fields show strong flow lines from in the negative x direction. In addition, as the time intervals increases, the average mean values gradually decreases, and flow fields become more varied.

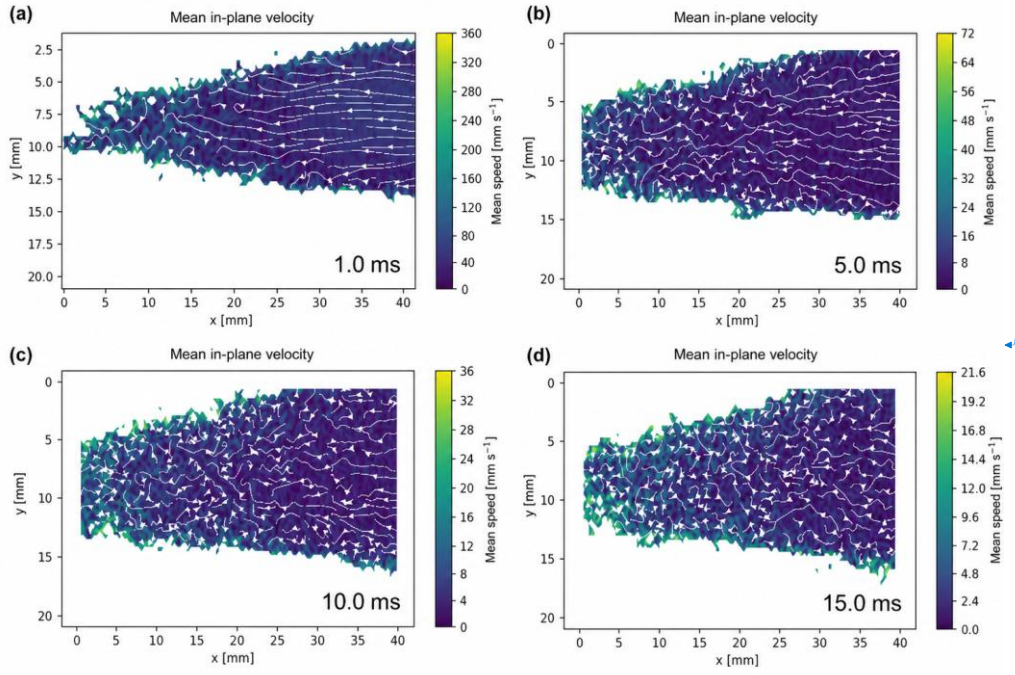


Figure S3: The following plot shows the time average velocity fields for different time intervals with the overall acquisition period kept longer than 10 seconds. A.) is for 1.0 ms, B.) is for 5.0 ms, C.) is for 10.0 ms, and (d) is for 15.0 ms. As the time interval increases more turbulent flows become present leading to a higher magnitude in velocity. Subsequently, the average value becomes more consistent in one direction as indicated by the streamlines.

Figure S4 shows the mean velocity per frame, and the cumulative mean over the duration of the measurement. As the time interval is increased the flow fields converge to a steady value faster. In addition, the mean field decreases as the time interval increases. This is attributed to longer intervals not capturing the turbulent dynamics that are present as the particles transverse in the -x direction of the cameras field of view. There is also not a continuous flow present in every frame which is captured by gaps in the data.

Formatted: Keep with next

Formatted: Normal

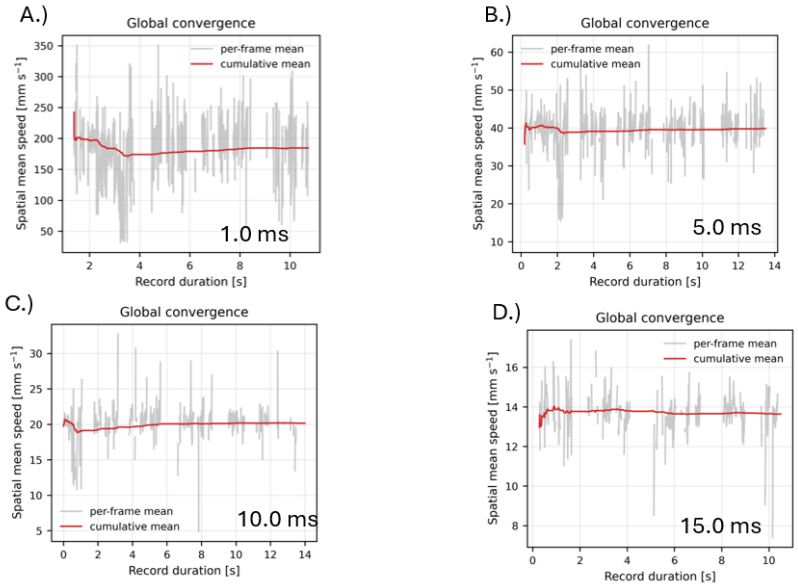


Figure S4 Shows the instantaneous velocity and convergence of the continuous mean values for different pseudo frame time intervals. A.) 1.0 ms, B.) 5.0 ms, C.)10.0 ms, and D.) 15.0 ms.

To better capture the turbulence nature of the fluid flow, Reynolds decomposition was applied. Reynolds decomposition separates each instantaneous velocity component into a mean and a fluctuating part, $u_i(x,t) = \bar{u_i}(x) + u_i'(x,t)$, where the overbar denotes a time average and the primed term captures the turbulent fluctuation about that mean. Applying this decomposition to the velocity field measured at each point allows the second-order statistics of the flow to be isolated from the mean advection. The covariance of the fluctuating velocity components, $\overline{u_i'u_j'}$, forms the Reynolds stress tensor and quantifies the degree to which fluctuations in different directions are correlated rather than independent. The diagonal terms ($\overline{u'^2}$, $\overline{v'^2}$) give the variance of the streamwise and wall-normal fluctuations and are directly related to the turbulent kinetic energy, while the off-diagonal term ($\overline{u'v'}$), the Reynolds shear stress, indicates the extent to which momentum is transported across the flow by turbulent motion; a nonzero value reflects a systematic correlation between streamwise and wall-normal fluctuations, as occurs when coherent turbulent structures sweep higher-momentum fluid toward the wall or ejected lower-momentum fluid away from it (Beresh et al., 2018). For the measured particle flows, it is observed that the covariance field are more prominent towards the end of the flow, then when exiting the nozzle.

Formatted: Keep with next

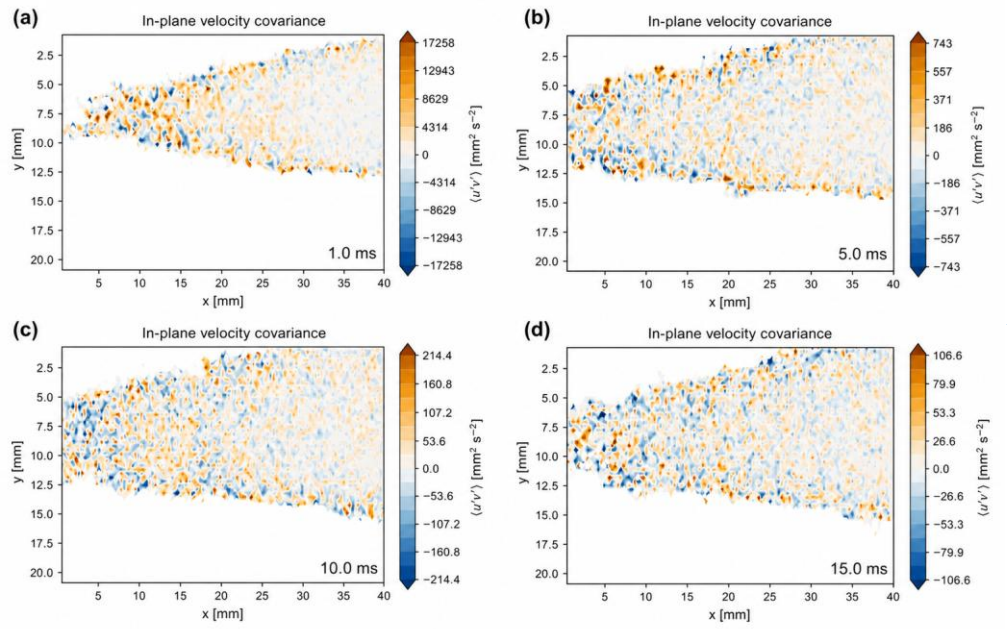


Figure S5 The following plots hows the velocity covariance from different time intervals. A.) is for 1.0 ms, B.) is for 5.0 ms, C.) is for 10.0 ms, and (d) is for 15.0 ms. As the time intervals increases the covariance across the flow decreases since the velocity fields become less apparent for longer time intervaa

Formatted: Keep with next